UC Berkeley
SEMM Reports Series

Title
Finite Element Formulation and Solution of Contact-Impact Problems in Continuum Mechanics - III

Permalink
https://escholarship.org/uc/item/5tg1s0qn

Authors
Hughes, Thomas
Taylor, Robert
Sackman, Jerome

Publication Date
1975-07-01

eScholarship.org Powered by the California Digital Library
University of California

Structures and Materials Research
Department of Civil Engineering

THIS REPORT IS AVAILABLE FROM:

NISEE/COMPUTER APPLICATIONS
379 DAVIS HALL
UNIVERSITY OF CALIFORNIA
BERKELEY CA 94720

(415) 642-5113

Report No. 75-7

FINITE ELEMENT FORMULATION AND SOLUTION OF CONTACT AND IMPACT PROBLEMS IN CONTINUUM MECHANICS -III

by

Thomas J. Hughes
Robert L. Taylor
Jerome L. Sackman

This report was prepared under subcontract number
N68305-75-C-0004

sponsored by

Civil Engineering Laboratory
Naval Construction Battalion Center
Port Hueneme, California

as part of Funding Document Number
ONR N00014-75-WR-5-0197

Funded by Office of Naval Research
Arlington, Virginia

July 1975

Table of Contents

Acknowledgement

This report was prepared under Subcontract No. N68305-75-C-0004; sponsored by Civil Engineering Laboratory, Naval Construction Battalion Center, Port Hueneme, California as part of Funding Document No. N00014-75-WR-5-0197 which was funded by the Office of Naval Research.

The opinions, findings and conclusions expressed in this publication are those of the authors and not necessarily those of the Civil Engineering Laboratory or the Office of Naval Research.

The authors would like to acknowledge the considerable contributions of Research Assistants Alain Curnier and Worsak Kanoknukulchai to the work reported upon herein.

Introduction

In this progress report we describe work completed thus far under Contract No. N68305-75-C-0004 (Proposal UCB-Eng.-3889). As we frequently allude to our previous work [1], [2] and [3], it will prove helpful to the reader to be somewhat familiar with these references.

In Section I we present several recently run check problems using the Hertzian contact-impact algorithm. These problems have helped us to increase the reliability of the Hertzian algorithm, demonstrate its accuracy and versatility with regard to a wide range of contact-impact problems, and delimit its range of applicability.

In Section II we describe our work in developing finite element models for nonlinear compressible, incompressible and nearly-incompressible elastic bodies. Our theoretical work in this area is completed, and implementation and check-out is currently in progress.

In Section III we present detailed algorithms for determining if, and where, contact has been made for the kinematically nonlinear case. This work builds upon the scheme initiated in [2]. Implementation of these algorithms in FEAP has commenced.

A simple dry friction contact theory is described in Section IV. The frictionless and no-slip extremes are special cases of this scheme. Algorithms are currently being designed for implementing this model in FEAP, and will be described in succeeding progress reports.

I. Recently Run Example and Check Problems Using the Hertzian Contact-Impact Algorithm

Several problems demonstrating the effectiveness of the Hertzian contact impact algorithm have been reported upon previously (see [2] and [3]). In this section we present the results of some recently run examples.

1. Head Injury Model

Several contact-impact analyses of an axisymmetric spherical head model were performed (see [22]). The model consists of a three-layered skull and encapsulated brain (Fig. I-1). The radius of the brain cavity R=2.95", the thickness of each hard bone layer is 0.05", and the thickness of the diploë layer is 0.10". Material properties are taken to be linear elastic and are given in Table I-1. Bilinear displacement finite elements were used to model the skull and brain. In the skull, three layers of elements were used through the thickness and four-point Gaussian quadrature was employed. The brain elements make use of one-point quadrature (so-called fluid elements).

a. Hollow skull contacting a rigid surface

The skull was discretized into 51 elements and 7 candidate contact elements were employed (see Fig. I-2a). The skull is fixed at the uppermost node and a rigid frictionless surface is pressed into it from the bottom. The rigid surface, initially just touching the skull, is given an upward motion of .1 inches per step until a total motion of .5 inches was achieved. Inertial effects were neglected.

Tracings of computer plotted deformed configurations and contact pressures (obtained from nodal contact forces by a tributary area method) are depicted in Fig. I-2b to 2f. Note how the peak contact

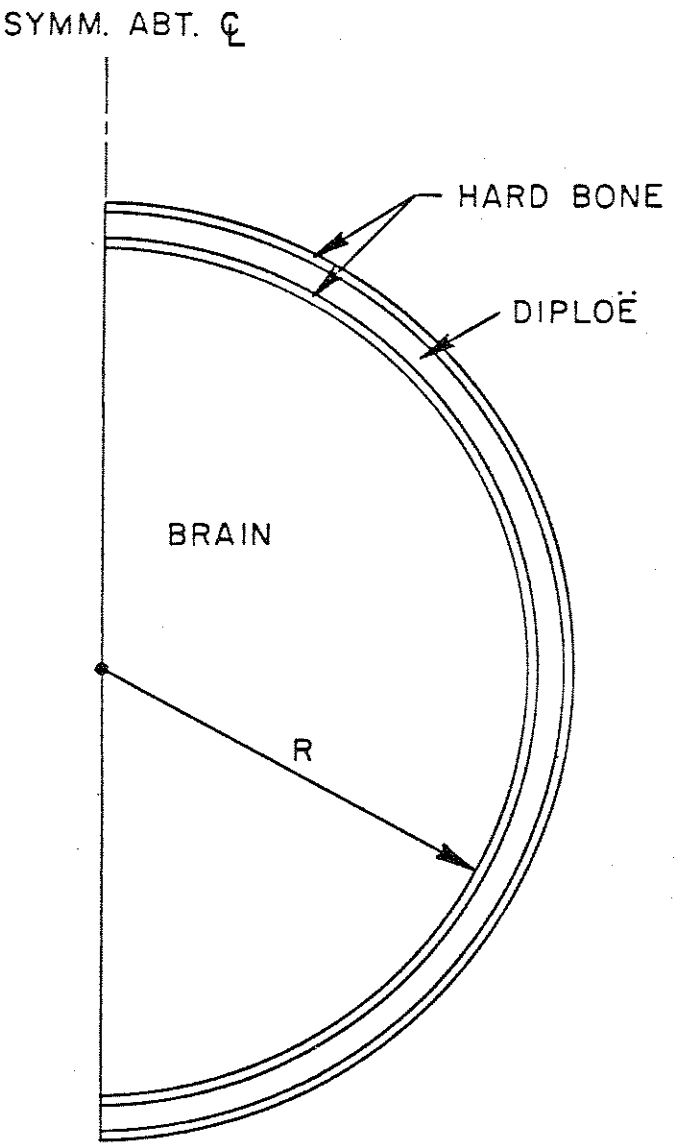

I-1 Axisymmetric spherical head injury model.

Table I-1. Material Properties for Head Injury Model

Property	Hard Bone	Diploë	Brain
K - Bulk Modulus (10^6 psi)	1.333	.1333	.305
G - Shear Modulus (10^6 psi)	.8	.08	.0305
ρ - Density (10^{-4} lb-sec^2/in^4)	2.	.2	.037

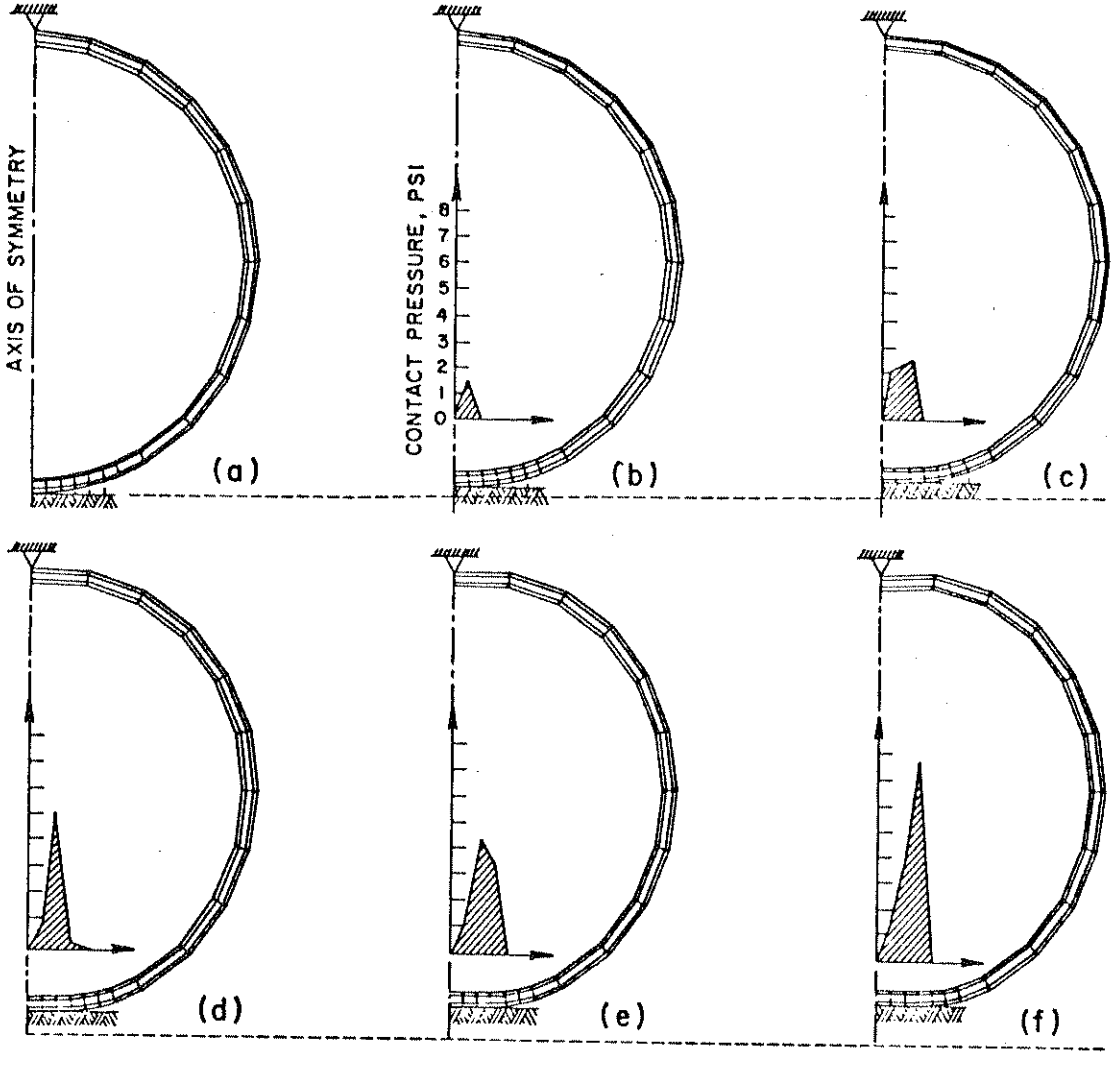

I-2 Initial (a) and deformed (b-f) mesh configurations of a hollow skull model contacting a rigid surface.

pressure occurs towards the outer radius of the contact zone. This is a common feature of shell-like contact phenomena, but quite opposite that for a homogeneous elastic sphere (see [2], Section I-1).

b. Hollow skull impacting a rigid surface

The mesh of the previous problem is also used here. The data are:

$\Delta t = .05 \times 10^{-5}$ sec (Time step)

$\beta = .25$, $\gamma = .5$ (Newmark parameters)

The uniform initial velocity of the sphere was 352.in/sec (=20 mph) downward. In this example we were interested in seeing the early-time wave propagation effects, and thus we employed a time step which is close to the transit time for a dilatational wave to travel through the thickness of each skull layer (the transit time for the hard bone layer equals $.0456 \times 10^{-5}$ sec). The contact force for the first 100 time steps is presented in Fig. I-3. The period of oscillation superposed upon the results is approximately $.35 \times 10^{-5}$ sec, which is very close to the time required for a dilatational wave to pass through the entire thickness of the skull and back (i.e., approximately $.365 \times 10^{-5}$ sec).

c. Impact of skull-brain model against a rigid surface

The mesh for this problem is depicted in Fig. I-4. The modeling of the skull portion is identical to the previous two cases. Here we used a time step of $.365 \times 10^{-5}$ sec; all other data are the same as for the previous case. Pressure profiles over the contact surface, obtained from the nodal contact forces by a tributary area method, are depicted in Fig. I-5. It is interesting to compare these results with the profiles obtained from the dynamic Hertz problem, [3], and the quasi-static shell problem, case a. In the former case, the peak contact

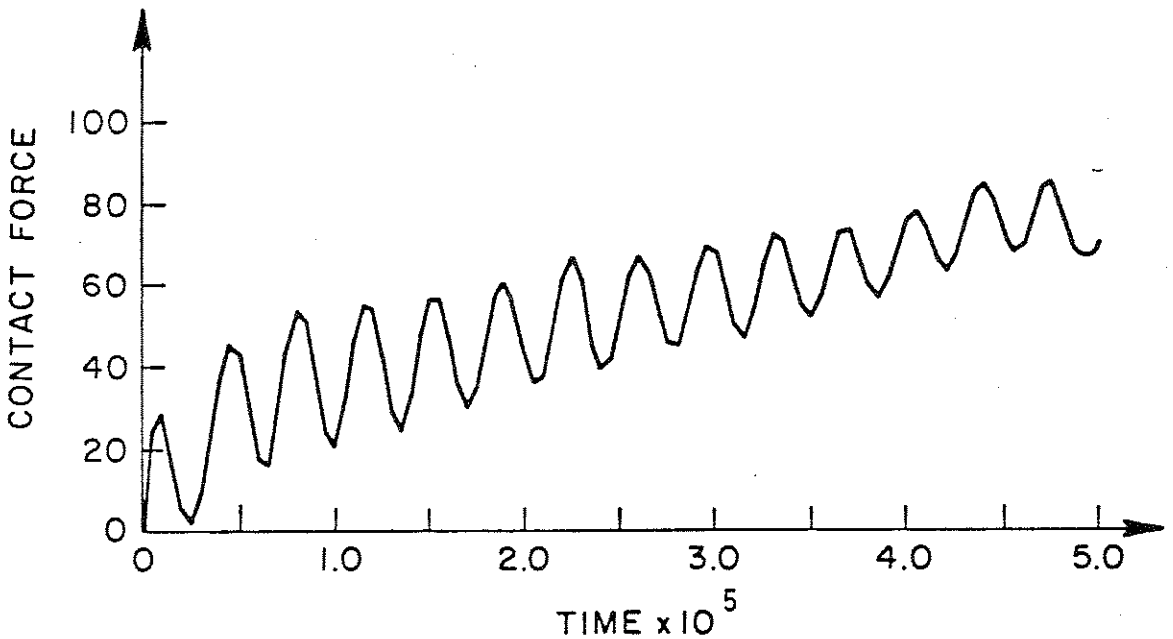

I-3 Contact force vs time for a hollow skull impacting a rigid surface.

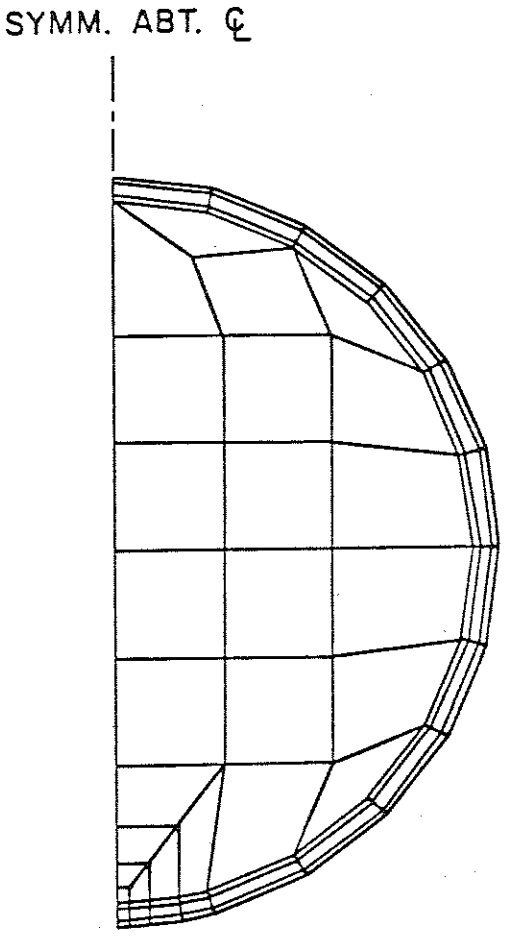

I-4 Finite element mesh for impact of skull-brain model against a rigid surface.

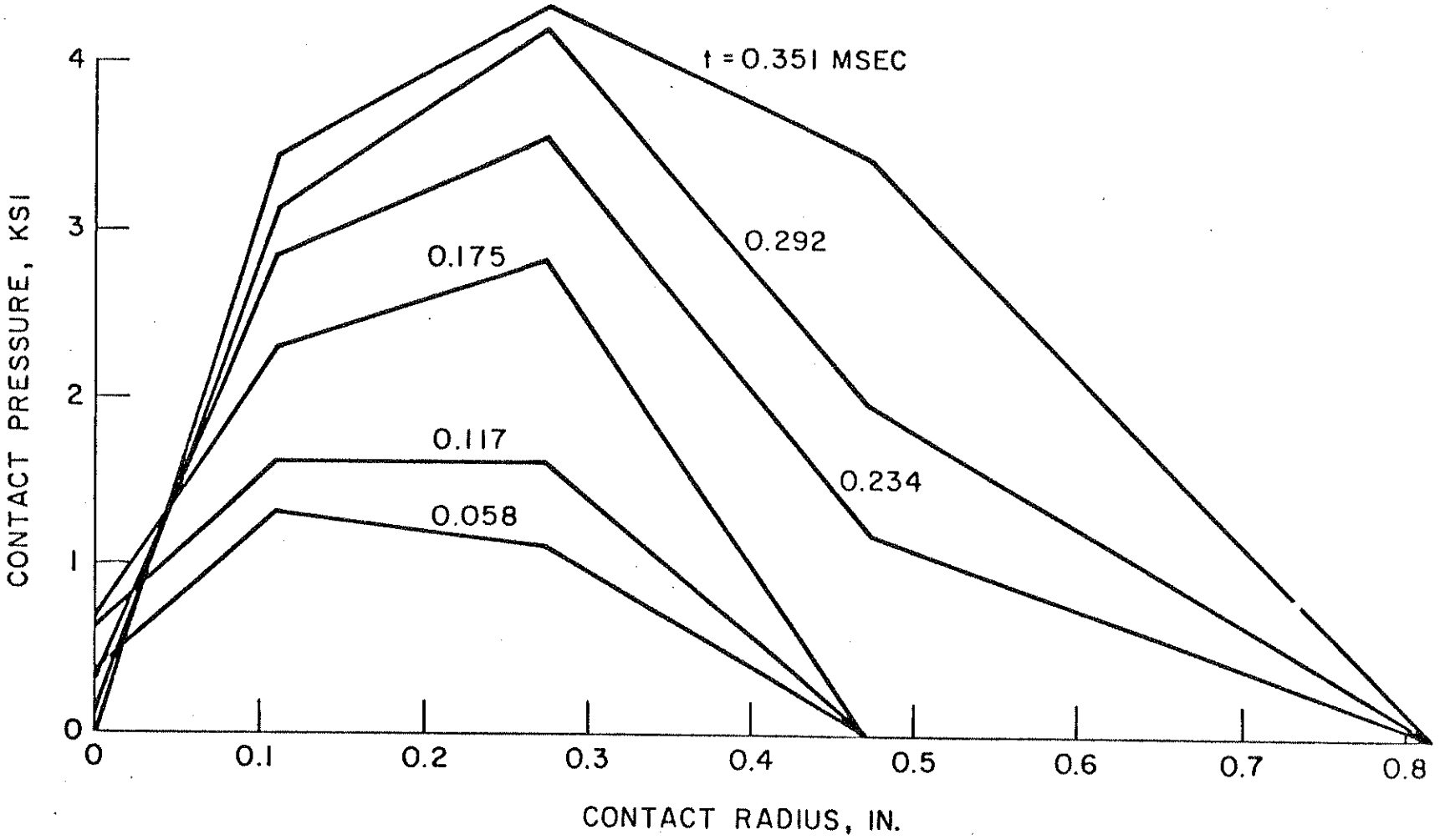

I-5 Contact pressure profiles for skull-brain impact problem.

pressure is located on the axis of symmetry, and in the latter case, it is towards the periphery of the contact zone, falling off to zero along the symmetry axis (cf. Fig. I-2). Here, Fig. I-5, results somewhere in between these extremes is achieved.

2. Rectangular Block Impacting a Rigid Surface

An analysis was performed of a plane strain linear elastic rectangular block impacting a rigid surface. The finite element mesh is shown in Fig. I-6. Data are:

$\rho = 0.1$ (Density)

$E = 1000.$ (Young's modulus)

$\nu = .3$ (Poisson's ratio)

$L = 9.$ (Length)

$\Delta t = .002725$ (Time step)

$\beta = .001001$, $\gamma = .502$ (Newmark parameters)

The time step is the transit time for a dilatational wave to propagate the length of one element. Initially the block is traveling at a uniform velocity of 1. (downward). The block impacts the rigid surface at t=0. Outside the shaded zone (see Fig. I-7) defined by R=ct, where c=366.9 is the dilatational wave velocity, the exact solution consists of two constant zones, I and II, separated by the dilatational wave front which emanates from the initial impact. The circular wave front is a result of reflections off the right-hand side (free) boundary.

We were interested in determining the early time results for this problem which can be compared with the known solution in zone II and provide a test of the discrete impact conditions. Eight time steps were run, allowing the front separating zone I from II to propagate to within

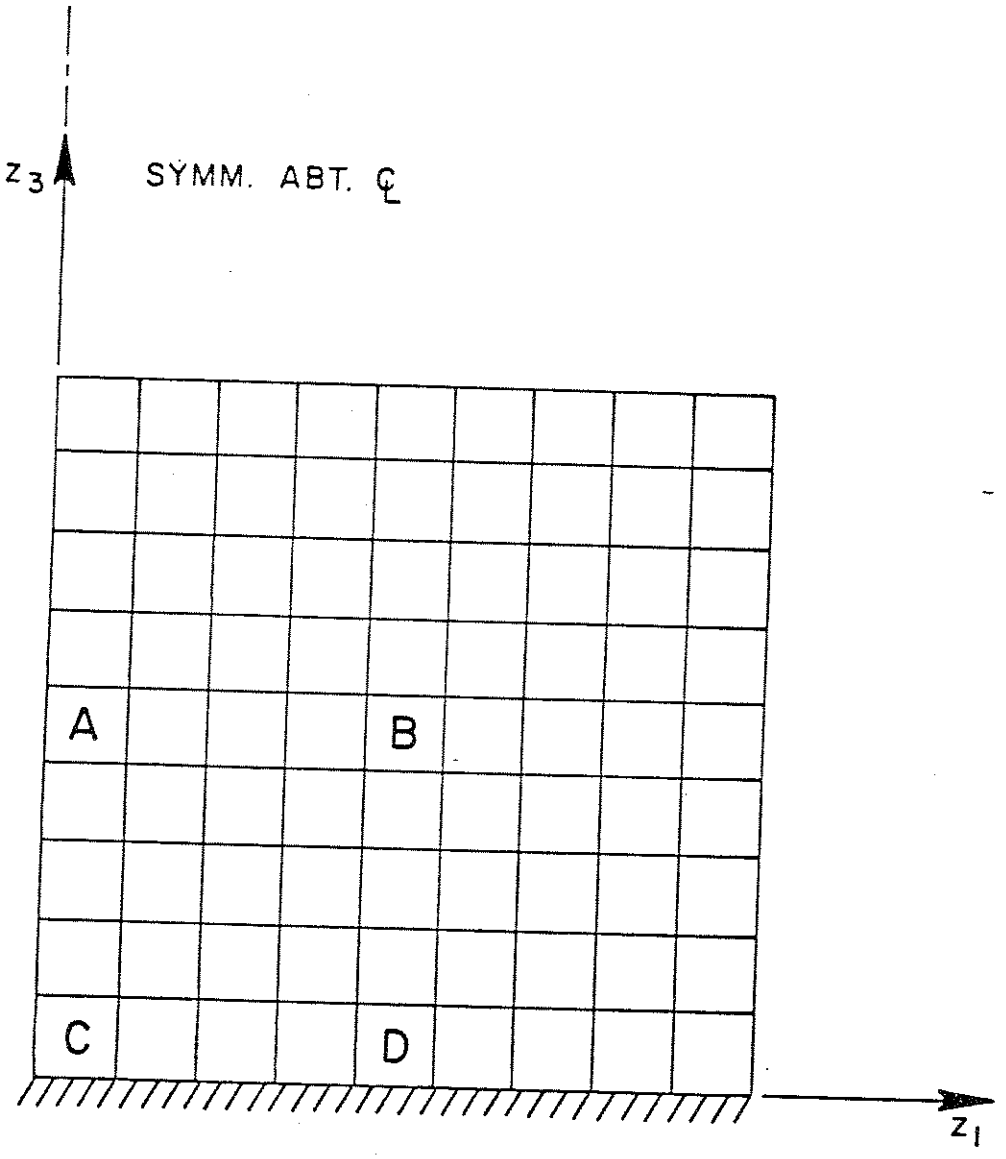

I-6 Finite element mesh for a plane strain rectangular block impacting a rigid surface.

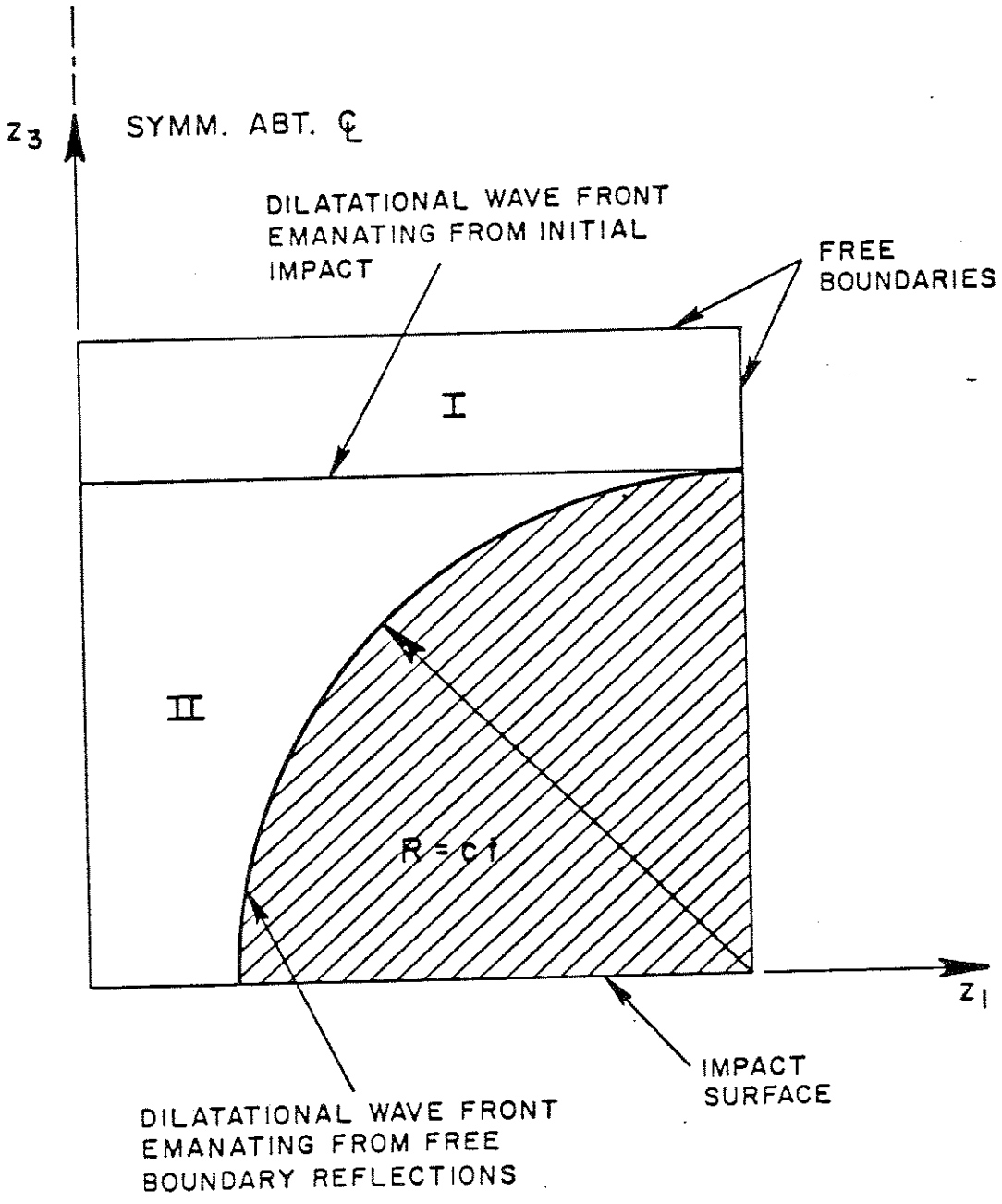

I-7 Wave front diagram for rectangular block impact problem.

one element length of the top surface. Stress results for several elements are depicted in Fig. I-8. In each case the rise of stress from zero to the exact value is achieved in one time step, and this value is maintained until the wave from the right-hand boundary reaches the element. The results corroborate the effectiveness of the discrete impact conditions.

A deformed mesh at t=.0163, with displacements magnified by a factor of 50., is superposed upon the undeformed mesh in Fig. I-9. At this time the plane front has traveled upward through 6 elements. Note that bulging along the right-hand side occurs up to this point. The effect of a frictionless contact surface is evidenced by the displacement to the right of the lower right-hand corner node.

3. Dynamic Rigid Punch Problems

a. Triangular punch

A rigid triangular punch is driven into a linear elastic half-plane at constant velocity V=100. (see Fig. I-10). Data are:

$\rho = .01$ (Density)

$E = 1000.$ (Young's modulus)

$\nu = .3$ (Poisson's ratio)

$\alpha = \tan^{-1} 2$ (Punch angle)

$\Delta t = .0025$ (Time step)

$\beta = .25$, $\gamma = .5$ (Newmark parameters)

Five contact elements were employed. The initial mesh configuration and several deformed configurations are illustrated in Fig. I-11.

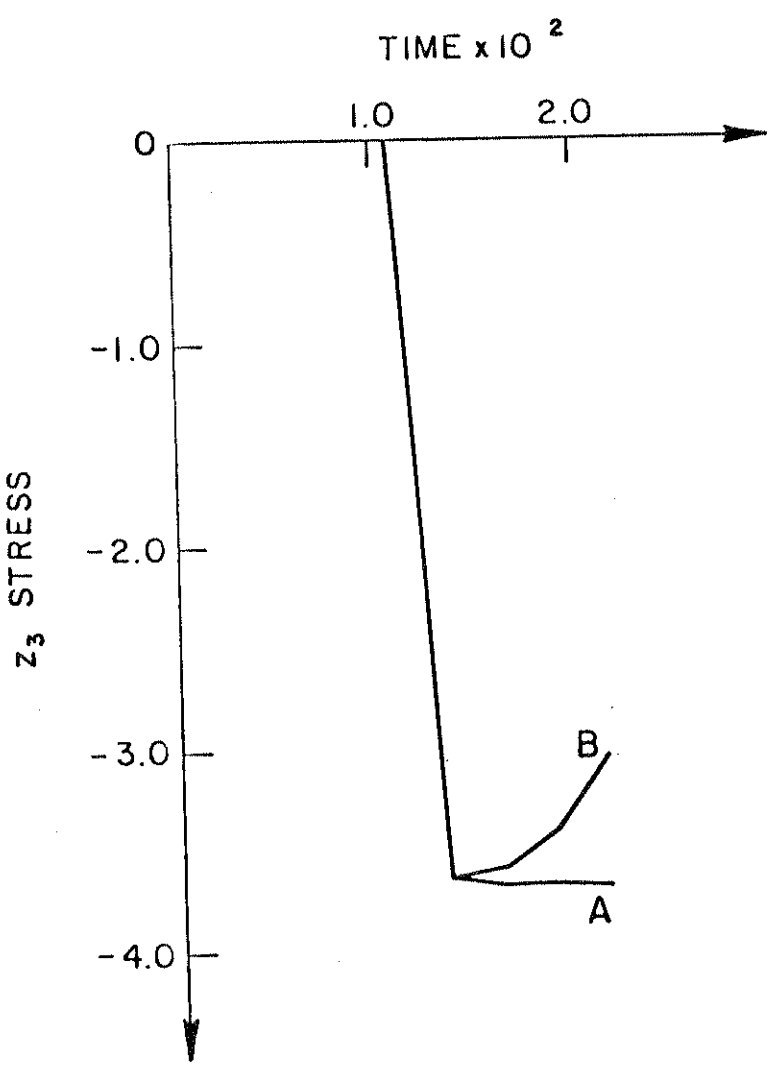

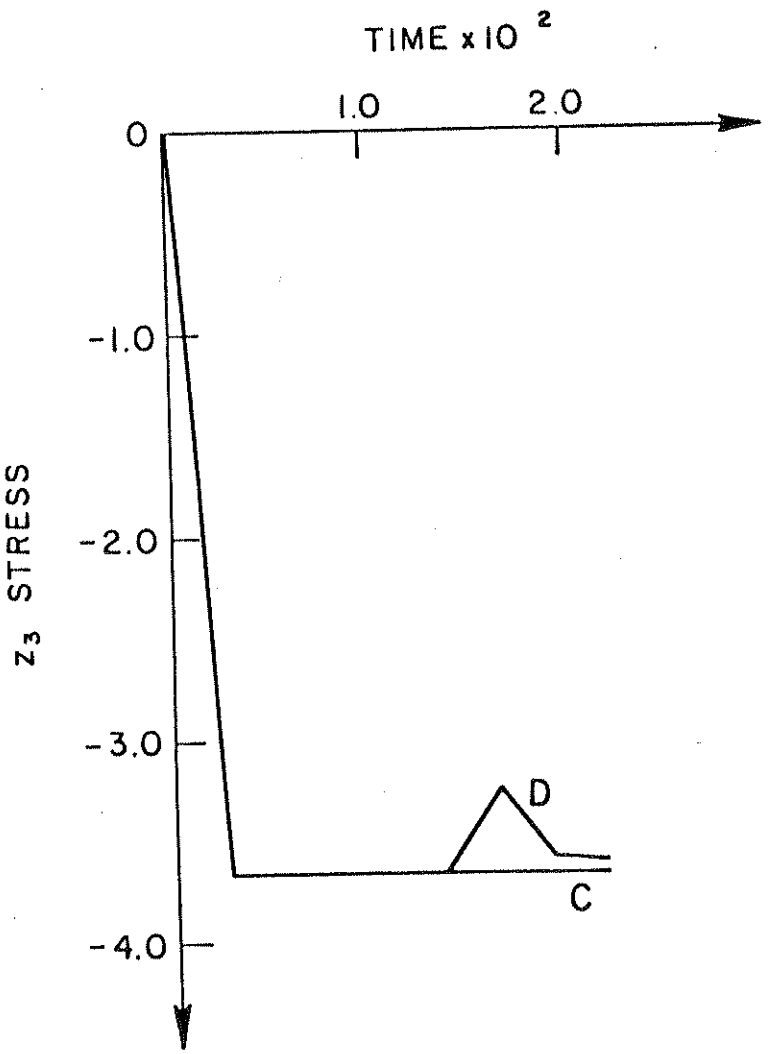

I-8 Stress results for rectangular block impact problem.

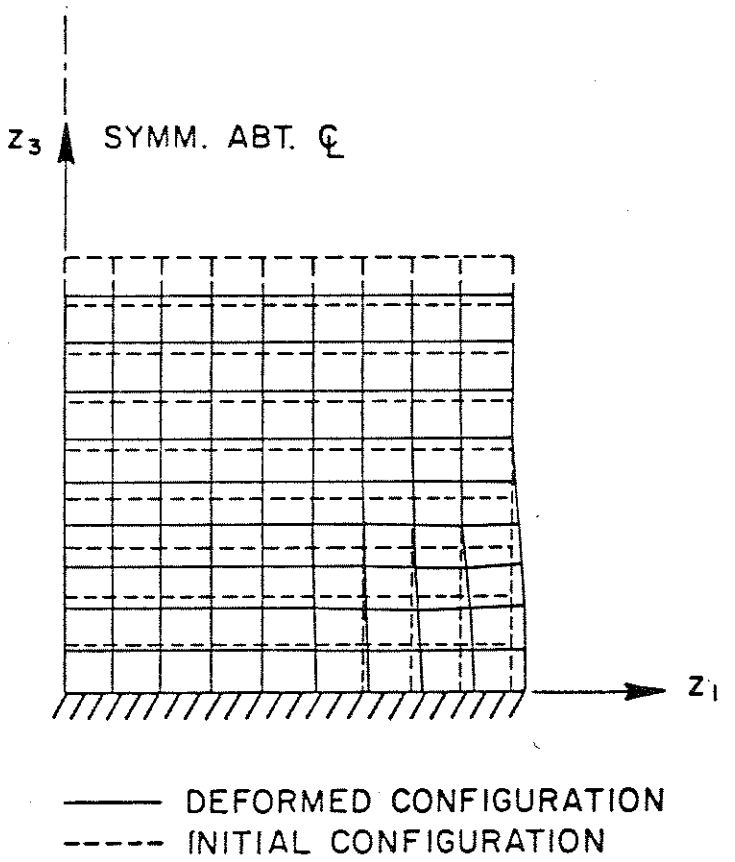

I-9 Deformed configuration superposed upon initial configuration for rectangular block impact problem at time .0163. The displacements are magnified 50 times.

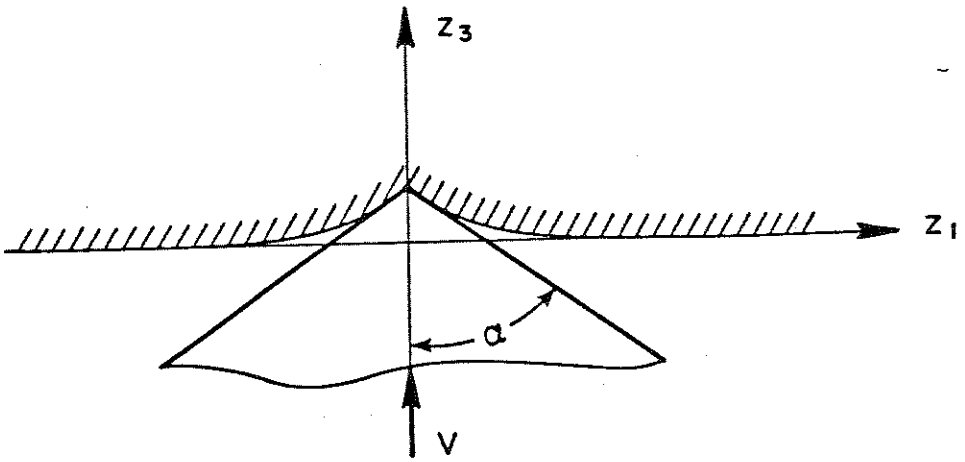

I-10 Rigid triangular punch driven into a half-plane at constant velocity V.

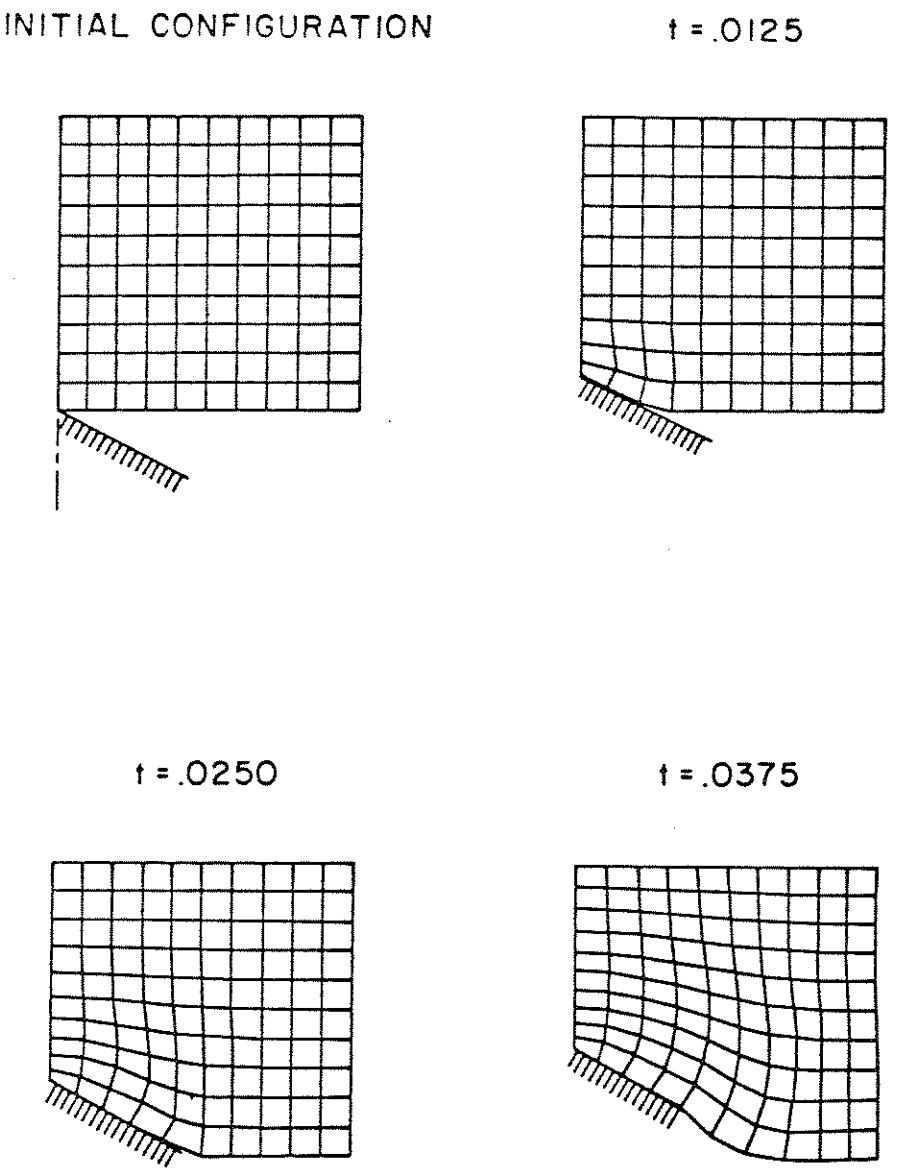

I-11 Initial and deformed configurations for rigid triangular punch problem.

b. Parabolic punch

A rigid parabolic punch was driven into the half-plane at a constant acceleration A = 4000. (see Fig. I-12). The surface of the punch is defined by the equation $z_3=z_1^2/8$. The remaining data are the same as in the previous case. The initial mesh configuration and deformed configurations are depicted in Fig. I-13.

Total contact force for cases a. and b. is known [20] to vary linearly and quadratically, respectively, with time. The results of the finite element analyses are seen to exhibit this behavior (see Fig. I-14).

The results for case b. employed a modification to the velocity impact conditions. Specifically, the velocities of the last time step prior to impact, $\dot{u}^{\alpha}_{-1}$, in Eq. $(II\text{-}8)_1$ of [2], were replaced by the velocities of the last iteration prior to impact, $\dot{u}^{\alpha}_{-}$. This was done because the impactor was accelerating, causing the velocities to vary linearly over the time step. Results using $(II\text{-}8)_1$ of [2] although showing the general trend of Fig. I-14, oscillated quite a bit before settling down. In general this artifice is not to be recommended; the sharp impact results of previous problems (namely, the bar problems presented in [2] and [3] and the block problem of the previous subsection) would not have been obtained if this was made the rule rather than the exception. What this problem does emphasize is that more sensitive (i.e., higher-order) impact and release conditions are necessary if one is to avoid taking excessively small time steps during the impact and release phases of a contact problem. The concept of higher-order impact conditions was alluded to in [3].

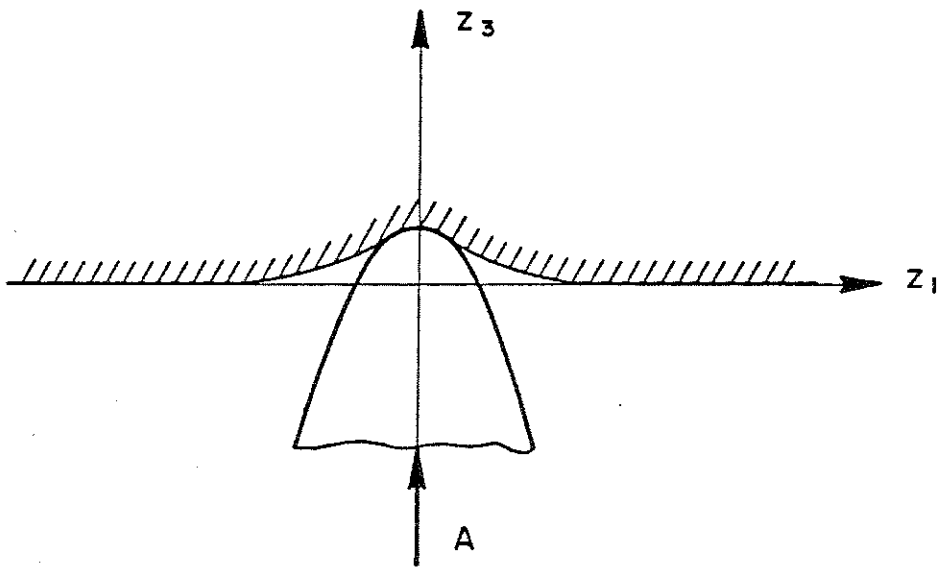

I-12 Rigid parabolic punch driven into a half-plane at constant acceleration A.

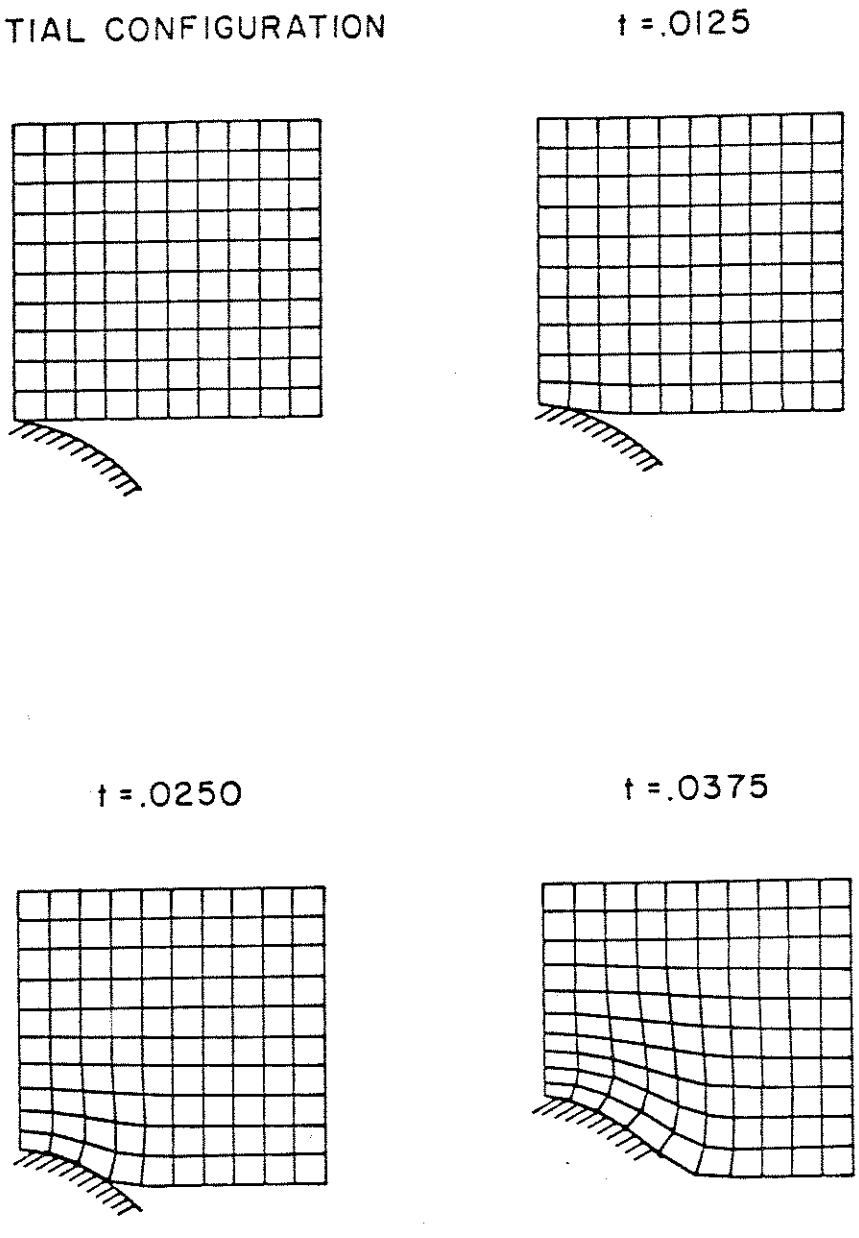

I-13 Initial and deformed configurations for rigid parabolic punch problem.

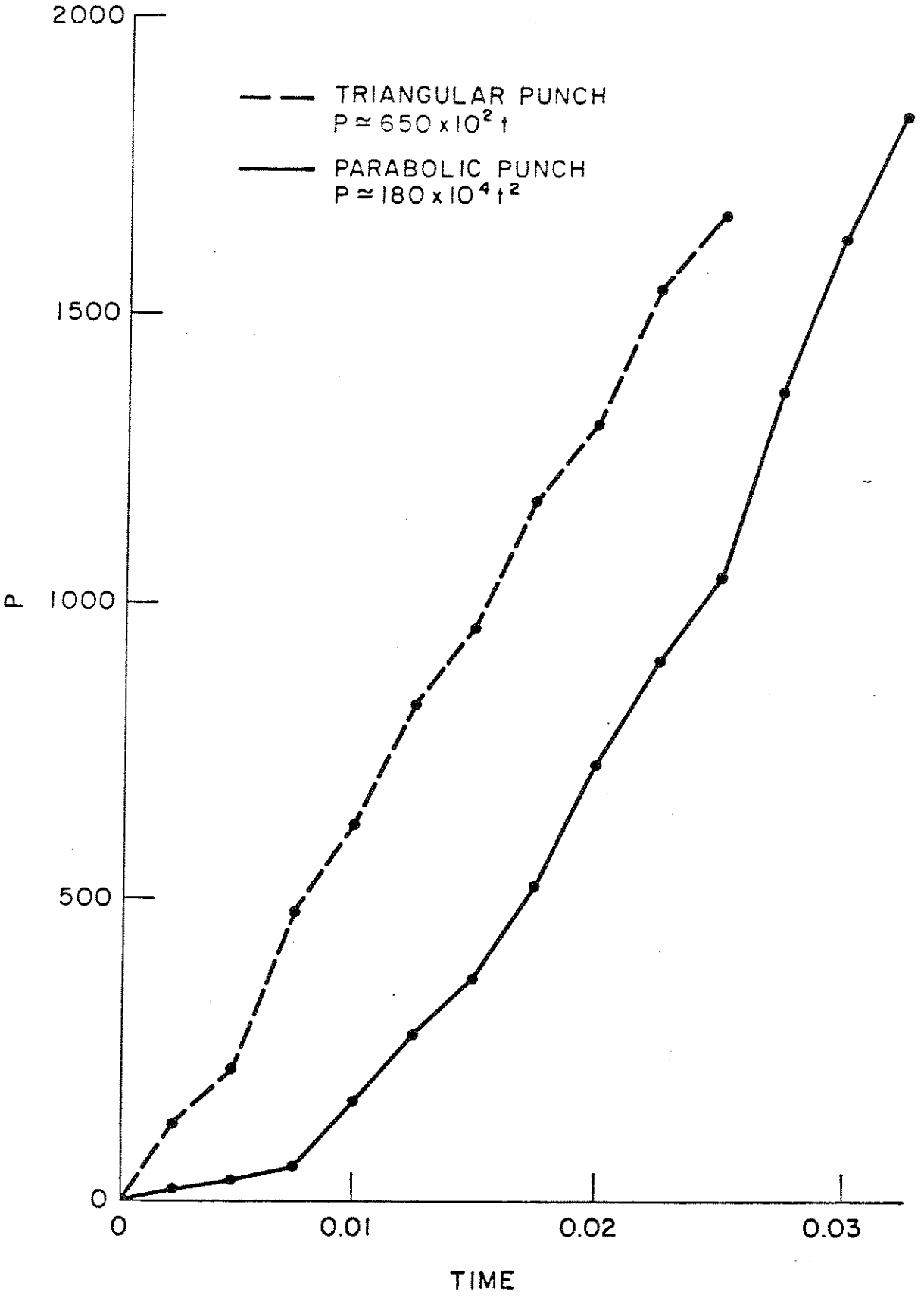

I-14 Total contact force vs time for rigid punch problems.

4. Static Analyses of Germanium Crystals

We have recently aided a research team of Berkeley physicists studying electron-hole drops in germanium (see for example [21]) by performing contact analyses of germanium crystals. Their work has been featured in lengthy articles in the San Francisco Chronicle 5/19/75, New York Times 5/19/75, and other major periodicals. Briefly, their theory indicates that long-lived electron-hole drops will occur around the point of maximum $\varepsilon_{11} - \varepsilon_{33}$, where ε_{ij} are the infinitesimal strains, in stressed germanium crystals. Their experimental technique enables them to photograph the electron-hole drop (see Fig. I-15). This was the first direct photographic evidence of the existence of this phenomenon.

The Hertzian contact algorithm was employed to calculate the strain contours of sample crystals. For example, the following data were employed to analyze the plane strain configuration illustrated in Fig. I-16.

Nylon set screw:

$$E = 1000. \quad \text{dynes/cm}^2$$

$$\nu = .3$$

Germanium crystal:

$$E = 13850. \quad \text{dynes/cm}^2$$

$$\nu = .3$$

The radius of the germanium crystal is 2 mm. The nylon set screw was driven into the crystal .08 mm, as illustrated in Fig. I-16, and five of the candidate contact nodes engaged. In Fig. I-16 we also show contours of $\varepsilon_{11} - \varepsilon_{33}$. The computed point of maximum $\varepsilon_{11} - \varepsilon_{33}$ is in close agreement with the photographed location of the electron-hole drop (cf. Fig. I-15).

I-15 First photograph of an electron-hole drop in germanium.

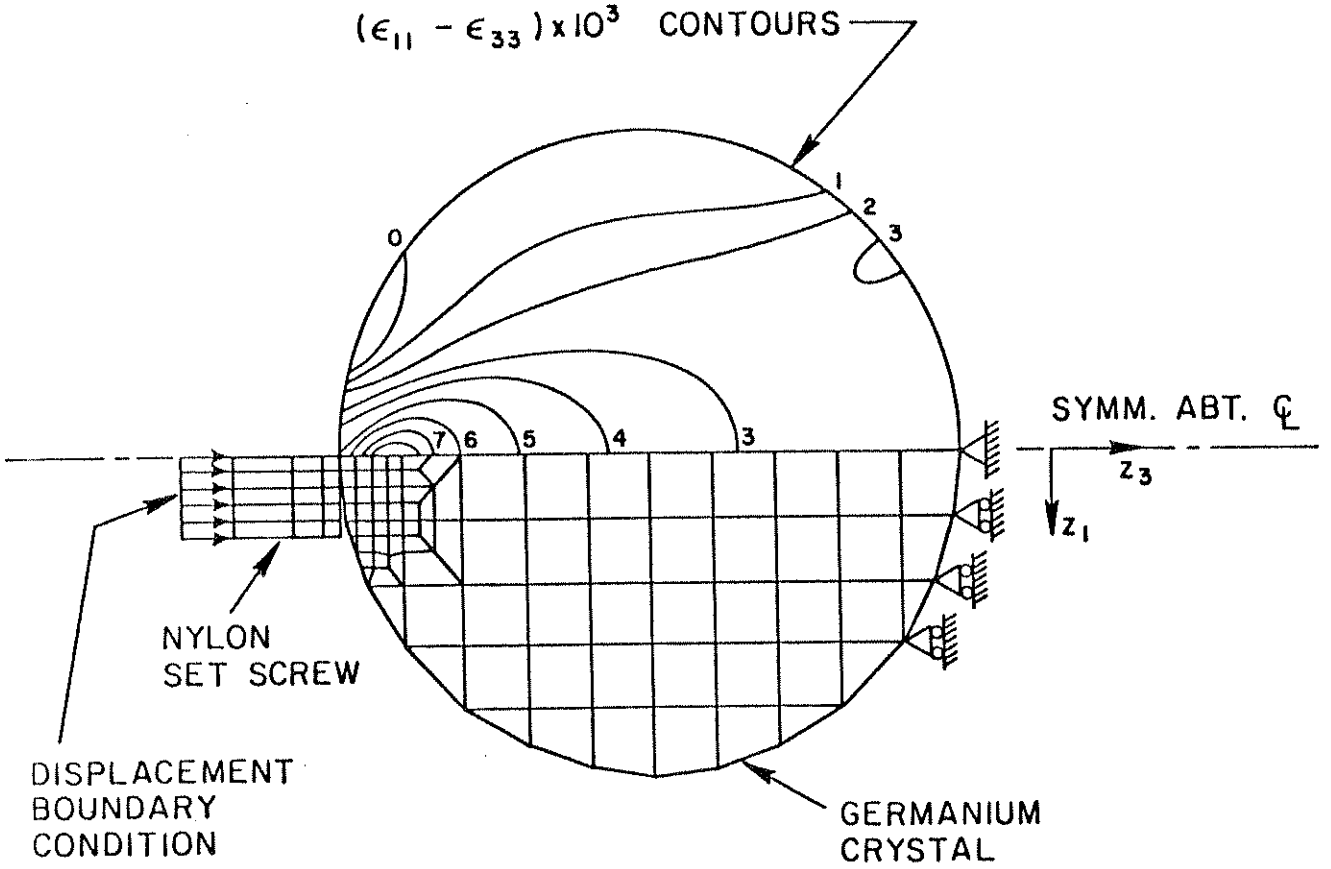

I-16 Finite element mesh and strain contours for contact analysis of a germanium crystal.

II. Analysis of Nonlinear Compressible, Incompressible and Nearly-Incompressible Elastic Bodies

1. Introduction

The finite element analysis of nonlinear phenomena in solid mechanics is presently an area of active research. Our algorithm for nonlinear contact-impact problems has been described in previous work (see Chap. II of [1], p. 46 of [2], and [3]). Although this algorithm is applicable to general nonlinear problems, thus far we have only considered nonlinearities attributable to the contact area development. In the present work we describe our formulation for nonlinear compressible, incompressible and nearly-incompressible elastic bodies. As is well known, the incompressible and nearly-incompressible cases require special care in the development of numerical formulations. The background for this problem and our approach are described in Section II-3. This work relies heavily on the formulation for the compressible case which we now proceed to describe.

2. Finite Element Formulation for Nonlinear Compressible Elastic Bodies

Recall form [1], [2] and [3] that it is only necessary to construct the mass matrix $\underset{\sim}{M}$, vector of elastic forces $\underset{\sim}{K}(\underset{\sim}{u})$, vector of external loads $\underset{\sim}{R}$, and tangent stiffness matrix $D\underset{\sim}{K}(\underset{\sim}{u})$ to perform nonlinear analysis. As in [1], we work in terms of the initial configuration B of the body in question. Our present notation is consistent with that of [1], Section 2, except that we work in terms of cartesian components for concreteness. Let ρ_o denote the density in the initial configuration and let A_T be that part of ∂B, the boundary of B, upon which tractions are prescribed. Let $\bar{T}_a$ represent the prescribed Piola-Kirchhoff tractions, F_a the extrinsic body force and $x_a = x_a(X_A, t)$ the position

at time t of the material particle located at X_A in the initial configuration. The deformation gradients are denoted by $x_{a,A}=\partial x_a/\partial X_A$ and $\Phi(x_{a,A})$ is the strain energy per unit volume of the initial configuration. Throughout we employ the summation convention with regard to repeated indices (e.g., $x_a y_a=x_1 y_1 + x_2 y_2+x_3 y_3$). A superposed dot indicates time differentiation holding X_A fixed (e.g., $\ddot{x}_a$ is the acceleration) and δx_a indicates the variation of x_a. Finally P_{Aa} represents the first Piola-Kirchhoff stress tensor.

Upon application of standard discretization procedures (see [4]), the quantities

$$\int_B \rho_o \ddot{x}_a \, \delta x_a \, dB, \tag{II-1}$$

$$\int_B P_{Aa} \, \delta x_{a,A} \, dB, \tag{II-2}$$

$$\int_B \rho_o F_a \, \delta x_a \, dB + \int_{A_T} \bar{T}_a \, \delta x_a \, dA \quad , \tag{II-3}$$

and

$$\int_B A_{AaBb} \, \Delta u_{a,A} \, \delta x_{b,B} \, dB, \tag{II-4}$$

where $A_{AaBb} = \partial^2\Phi/\partial x_{a,A} \, \partial x_{b,B}$ is the elasticity tensor and Δu_a are displacement increments, correspond to $\underset{\sim}{M}\ddot{\underset{\sim}{u}}$, $\underset{\sim}{K}(\underset{\sim}{u})$, $\underset{\sim}{R}$ and $DK(\underset{\sim}{u})\cdot\Delta\underset{\sim}{u}$ respectively. Thus for a given elastic material (characterized via $\Phi(x_{a,A})$, say) the quantities $P_{Aa}=\partial\Phi/\partial x_{a,A}$ and A_{AaBb} can be determined and programmed into a finite element computer code. All other aspects of the analysis are standard and need not be considered further here.

We note that all geometric and material nonlinearities are encompassed in this simple formulation.

3. Finite Element Formulation for Nonlinear Incompressible and Nearly-Incompressible Elastic Bodies

When one passes to the incompressible limit in the theory of elasticity, a special formulation is required (see Truedell and Noll [5] for background). A pressure-like variable is introduced as an unknown and, concomitantly, an additional equation, restricting the motion to be isochoric, must be satisfied. The pressure-like variable is interpreted as the force which maintains this constraint.

In principle, the usual formulation of nonlinear elasticity covers all other unconstrained cases. However, it has been discovered in the application of finite element methods that, for nearly-incompressible cases,* numerical problems are encountered with the usual formulation of the theory. Within the context of the linear theory, these problems have been dealt with in two ways.

The first method is to reformulate the linear equations for the compressible case in a way reminiscent of the incompressible case (see Herrmann and Toms [6], Herrmann [7], Taylor, Pister and Herrmann [8], Key [9], and Hughes and Allik [10] for background and applications along these lines). What one does is to consider the stress a function of the strain and a mean-pressure variable. The constitutive equation relating the dilatation to the mean-pressure variable then must be satisfied independently. With a judicious choice of interpolation functions for the displacements and mean pressure, an effective numerical scheme can

---

* An example of how one may characterize the nearly-incompressible case is provided by assuming $.45 < \nu < .5$, where ν is Poisson's ratio, in classical isotropic elasticity.

be developed. This approach is equally valid for the compressible and incompressible cases. The variational formulation of this theory may be viewed as a special case of Reissner's theorem, since only a part of the stress (i.e., the mean pressure) is considered to be independent. We wish to emphasize here that this formulation, although capable of yielding successful numerical algorithms, is no panacea. This fact, although known for some time, does not seem to be widely appreciated. If one is naive in the use of this method it can lead to results equally bad as those obtained by the standard formulation. What one must do is employ "inconsistent" interpolation functions for the displacements and mean pressure to avoid degenerating to the standard formulation (see [10] for elaboration and numerical examples). This method has been used successfully on a wide range of engineering problems (see [6]-[10] and references therein).

Recently, Fried [11] has provided insight into what goes wrong with the usual formulation for the linear isotropic case. As a remedy he suggests using "inconsistent" numerical integration rules for the deviatoric and dilatational parts of the strain energy. This technique brings about a similar end as that of the "inconsistent" interpolation functions used in conjunction with the previously described formulation. Computations performed by Naylor [12] yield results consistent with Fried's theory.

In the nonlinear case similar numerical problems are anticipated. Thus alternative formulations are called for (see Oden [13], Iding, Pister and Taylor [14], and Argyris, Dunne, Angelopoulos and Bichat [15], for work already done in this area). The natural thing to do is to attempt generalizations of the methods described above. Our original intention

was to do this for the mean-pressure-variable formulation (see [16]). However, in the course of developing this method, we have become convinced that it is advantageous instead to adopt a generalization of the approach proposed by Fried. We do this for practical rather than theoretical reasons as either approach is, in principle, capable of handling the nearly-incompressible and incompressible cases. The main practical advantage of Fried's idea is that is involves only a minor (but delicate!) modification of the usual displacement formulation for the compressible case and thus results in a smaller system of equations than that associated with the mean-pressure-variable formulation. The computational effort saved because of this promises to be considerable in nonlinear analysis. In addition, the tangent stiffness matrix (for the non-contact case) is positive definite in a stable configuration, whereas in the mean-pressure-variable formulation it is always indefinite.

Our generalization of Fried's idea for the nonlinear case turns out to be extremely easy to implement. On the other hand, the mean-pressure-variable formulation poses some potentially insurmountable implementation problems.

We will first describe how the nearly-incompressible case can be handled within the general scheme of Section 2, then show how incompressible problems can be reduced to nearly-incompressible ones.

To discuss the nearly-incompressible case it is convenient to introduce a specific constitutive equation. Consider a strain energy function defined by

$$\Phi = 1/2\ \lambda(\ln J)^2 + \mu\, E_{AB}E_{AB}, \qquad \text{(II-5)}$$

where λ and μ are material parameters, $J=\det(x_{a,A})$ and $E_{AB}=1/2(C_{AB}-\delta_{AB})$ is the Lagrangian strain tensor, in which $C_{AB}=x_{a,A}x_{a,B}$ and δ_{AB} is the Kronecker delta. The first and second Piola-Kirchhoff stress tensors, corresponding to Φ, are given by

$$P_{Aa} = \frac{\partial \Phi}{\partial x_{a,A}} = \lambda(\ln J)X_{A,a} + 2\mu\, E_{AB}\, x_{a,B}, \qquad \text{(II-6)}$$

and

$$S_{AB} = \frac{\partial \Phi}{\partial E_{AB}} = \lambda(\ln J)\underset{\sim}{C}^{-1}{}_{AB} + 2\mu\, E_{AB}\,, \qquad \text{(II-7)}$$

respectively, where $^{*}(X_{A,a}) = (x_{a,A})^{-1}$ and $(\underset{\sim}{C}^{-1}{}_{AB}) = (C_{AB})^{-1}$. The elasticity tensor corresponding to Φ is given by

$$A_{AaBb} = \lambda(X_{A,a}X_{B,b} - (\ln J)X_{A,b}X_{B,a}) + \mu(\delta_{AB}x_{a,C}x_{b,C} + x_{b,A}x_{a,B} + 2\delta_{ab}E_{AB})\,. \qquad \text{(II-8)}$$

The following features make this model useful for evaluating the effectiveness of the nearly-incompressible finite element procedure to be described subsequently:

(i) It is isotropic with respect to the reference configuration (this can be seen by replacing $x_{a,A}$ in the definition of Φ by $x_{a,B}Q_{BA}$, where Q_{BA} is an orthogonal tensor, and observing that $\Phi(x_{a,A}) = \Phi(x_{a,B}Q_{BA})$).

---

* We use the notation (a_{ij}) to denote the matrix whose components are a_{ij}.

(ii) The linearized approximations of the constitutive equations (II-6) and (II-7) about the initial configuration yield the familiar relation of classical linear isotropic elasticity; namely

$$T_{ab} = \lambda \varepsilon_{cc} \delta_{ab} + 2\mu \varepsilon_{ab} ,$$

in which T_{ab} represents the Cauchy stress tensor and ε_{ab} the infinitesimal strain tensor.

(iii) The parameter λ allows continuous control of the compressibility. As $\lambda \to \infty$, the boundary value problem in question approaches one for which the material is incompressible (i.e., $J \equiv 1$). This permits numerical experiments over the entire range of compressibility. We shall explicate this further when discussing the incompressible case.

(iv) The model is extremely simple and properly invariant with respect to rigid motions.

We say this model exhibits compressible behavior when λ and μ are of the same order of magnitude. When λ is an order of magnitude, or more, greater than μ we say this model exhibits nearly-incompressible behavior. In the latter case, standard finite element formulations become ill-behaved. A heuristic reason for this is as follows. When λ is large, the motion of a finite element is restrained to be almost volume preserving. Thus a finite number of constraints are imposed upon the freedom of each element. Upon assembling the elements the total number of constraints generally exceeds the total number of degrees of freedom, thus causing a "locking" of the structure (see Nagtegaal, Parks and Rice [17] and Argyris et al. [15] for concrete examples of

this phenomenon). The obvious remedy is to reduce the number of constraints per element. The simplest way of achieving this for the material defined by (II-5) is to use lower-order quadrature formulas for the terms in (II-2) and (II-4) involving λ.

For example, consider the standard isoparametric four-node quadrilateral (see [4] for details). Whereas 2x2 Gaussian quadrature is generally used for this element, in the present circumstances only one-point quadrature (the centroid) should be used for the λ terms. This results in only one constraint upon the motion of the element and thus near-incompressibility is satisified in the mean. The behavior of this element should be similar (if not identical) to the constant mean pressure-bilinear displacements model, employed with success by Hughes and Allik [10]. One-point quadrature could be used for all terms if the appearance of the "keystone" mode [22], also known as the "hour-glass" mode, could be prevented.

Thus for constitutive models for which there exists identifiable parameters such as λ, which impose constraints upon the motion, under-integrating the λ terms remedies the locking which occurs in finite elements.

For the eight-node serendipity element (see Zienkiewicz, Taylor and Too [18]), 2x2 Gussian quadrature for all terms is anticipated to yield good results for the nearly-incompressible case. Thus this element is suitable for cases in which there is no easily identifiable parameter such as λ.

On the other hand, if it is desired to use the four-node element in conjunction with a material without an easily identified incompressibility parameter, then a slightly more general strategy must be adopted.

The idea again is to release some of the constraints within the element. This can be done as follows. Let the volume preserving part of $x_{a,A}$ be denoted by $\hat{x}_{a,A}$, i.e.,

$$\hat{x}_{a,A} = J^{-1/3} x_{a,A}; \tag{II-9}$$

clearly $\det(\hat{x}_{a,A}) = 1$. Then split the integrands of (II-2) and (II-4) in the following way:

$$P_{Aa}\ \delta x_{a,A} = J^{1/3}\ P_{Aa}\ \delta\hat{x}_{a,A} + \frac{1}{3}\ \delta x_{b,b}\ P_{Aa}\ x_{a,A}\ ,$$

$$\begin{aligned} A_{AaBb}\ \Delta u_{a,A}\ \delta x_{b,B} &= J^{2/3}\ A_{AaBb}\ \Delta\hat{u}_{a,A}\ \hat{\delta x}_{b,B} \\ &\quad + \frac{J}{3}^{1/3}\ \Delta u_{c,c}\ A_{AaBb}\ x_{a,A}\ \delta\hat{x}_{b,B} \\ &\quad + \frac{J}{3}^{1/3}\ \delta x_{c,c}\ A_{AaBb}\ \Delta\hat{u}_{a,A}\ x_{b,B} \\ &\quad + \frac{1}{9}\ \Delta u_{c,c}\ \delta x_{d,d}\ A_{AaBb}\ x_{a,A} x_{b,B}\ , \end{aligned}$$

where

$$\delta\hat{x}_{a,A} = J^{-1/3}\ (\delta x_{a,A} - \frac{1}{3}\ \delta x_{b,b}\ x_{a,A})\ ,$$

$$\Delta\hat{u}_{a,A} = J^{-1/3}\ (\Delta u_{a,A} - \frac{1}{3}\ \Delta u_{b,b}\ x_{a,A})\ .$$

Wherever J appears after the decomposition (II-9) is employed (e.g., in P_{Aa} or A_{AaBb}) replace it by lower-order interpolation. The same process should be carried out for $\Delta u_{a,a}$ and $\delta x_{a,a}$. For the four-node quadrilateral element, these quantities should be set equal to

their values at the centroid. Thus even for the most complicated material model numerical integration techniques can be employed effectively for the case of near incompressibility.

We will now show how the incompressible case may be reduced to the nearly-incompressible case. The constitutive equation for an incompressible material is given by

$$P_{Aa} = -p\, X_{A,a} + \hat{P}_{Aa},$$

or

$$S_{AB} = -p\, \underset{\sim}{C}^{-1}_{AB} + \hat{S}_{AB}, \tag{II-10}$$

where $\hat{P}_{Aa}$ and $\hat{S}_{AB}$ depend only on the motion. The variable p is to be determined by way of the solution to the boundary-value problem, which takes the form

$$\begin{aligned}
P_{Aa,A} + \rho_o F_a &= \rho_o \ddot{x}_a && \text{in } \mathcal{B},\\
J &= 1 && \\
N_A P_{Aa} &= \bar{T}_a && \text{on } \mathcal{A}_T,\\
x_a &= \bar{x}_a && \text{on } \mathcal{A}_x,\\
x_a &= x_{oa} && \text{in } \mathcal{B},\\
\dot{x}_a &= v_{oa} && \text{in } \mathcal{B},
\end{aligned}$$

where P_{Aa} is defined by $(II\text{-}10)_1$, N_A represents the unit outward normal to $\partial\mathcal{B}$, $\mathcal{A}_x$ is that part of $\partial\mathcal{B}$ upon which the motion is prescribed to be $\bar{x}_a$, $x_{oa}=\delta_{aA}X_A$ represents the initial positions of the points in $\mathcal{B}$ and v_{oa} is the given initial velocity. We wish to replace this

problem by a nearly-incompressible one. To do this we satisfy the condition J=1 by replacing p by $-\lambda \ln J$. Then for each λ the problem we solve fits into the forma⁺ of the nearly-incompressible case. Selecting λ appropriately depends upon the finite elements being used, the mesh and material properties (see Fried [11] for a discussion). Since $\ln J = -p/\lambda$, as $\lambda \to \infty$, $\ln J \to 0$, implying $J \to 1$. In an analysis, an acceptable compressibility error can be achieved by picking λ several orders of magnitude (say 3 or 4) larger than other material properties (e.g., μ in (II-5)).

III. Algorithm for the Two-Dimensional Kinematically Nonlinear Contact-Impact Problem

1. Introduction and Basic Ideas

Static and dynamic aspects of the Hertzian algorithm have been treated in [1], [2] and [3]. In [2] we described the basic ideas of the kinematically nonlinear scheme; namely, the form of the contact element matrices and the structure of the global matrices. In the present section, we extend these developments by describing the detailed algorithm for deciding when, and where, contact has been made for the two-dimensional case. Due to its geometric simplicity, only very simple logic is required to attain this end in the Hertzian case (see for example pp. 33-34 of [2]). However, in the kinematically nonlinear case the geometry is much more complicated and one must proceed more systematically.

We first review some of the basic notions introduced in [2], Section III-3. We assume that there are N^1 (N^2, respectively) candidate contact nodes associated with body 1 (2, resp.). Without loss of generality, we assume $N^1 \leq N^2$. To each of the candidate contact nodes of body 1, we assign a contact force vector $\underset{\sim}{\tau}_i$, $i=1,2,\ldots,N^1$. These are to be interpreted in the same way as in the Hertzian case, i.e., the $\underset{\sim}{\tau}$ vector field consists of Dirac delta functions located at the nodal points of body 1.

In the present work, we shall call body 1 the contactor (or impactor) and body 2 the target. We assume the target consists of a finite number of open, or closed, directed segments (see Fig. III-1). If the total number of segments equals n, then we must have

$$N^2 = \sum_{i=1}^{n} N_i^2 \ .$$

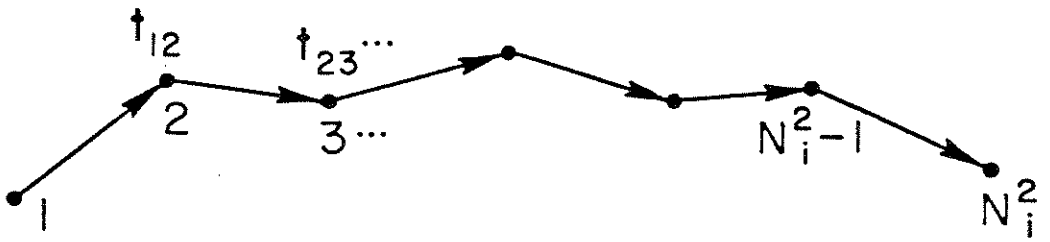

i TH OPEN TARGET SEGMENT

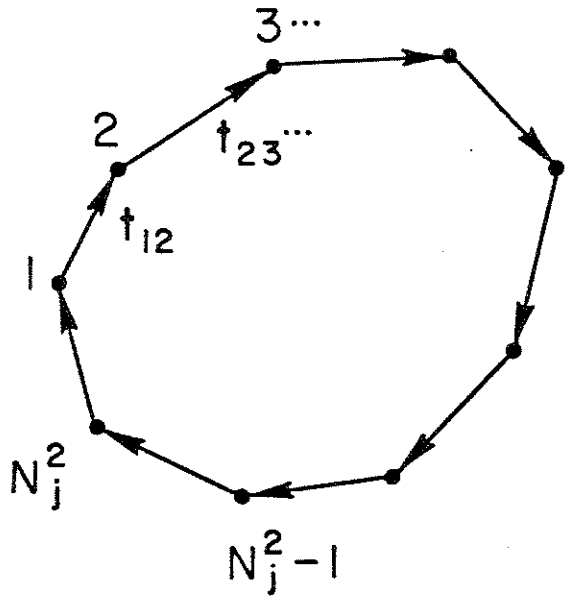

j TH CLOSED TARGET SEGMENT

III-1 Typical target segments.

The nodes of the i^{th} segment are connected by straight lines (element boundaries) in the fashion 1 to 2, 2 to 3,..., N_i^2-1 to N_i^2. In case the i^{th} segment is closed, nodes N_i^2 and 1 are also connected by a straight line, whereas if it is open they are not. For an open segment, nodes 1 and N_i^2 are called boundary points, and nodes 2,..., N_i^2-1 are called interior points. For a closed segment all nodes are classified as interior points. We lay down the restriciton that each segment must contain a minimum of three nodes.

The direction of the i^{th} segment is defined as follows. Let 1 and 2 denote the first two nodes of the segment. The vector $\underset{\sim}{t}_{12}$ connecting 1 to 2 and pointing towards 2 defines the direction of the entire segment. The direction of a segment enables us to determine whether a candidate contact point has penetrated the target. The details of this procedure are treated in the next section.

2. Logic for Determining if a Contact Point Penetrates a Target Segment

After each iteration in an analysis we must determine whether or not any candidate contact nodes have penetrated a target segment. Let P denote the location of candidate contact node k in $\{1,\ldots,N^1\}$, and let Q,R,S denote the locations of consecutive target nodes ℓ-1, ℓ, ℓ+1, where ℓ designates an interior node of some segment. We assume that the entire list of interior target nodes has been searched and k is found to be the closest to ℓ at the end of the i^{th} iteration during some time step (see Fig. III-2). Henceforth we will use superscripts to indicate iteration numbers. Thus $||P^i-R^i||$ is the minimum distance between P^i and all interior target nodes. For P^i the interior of the target is defined to be that part of the plane consisting of the two

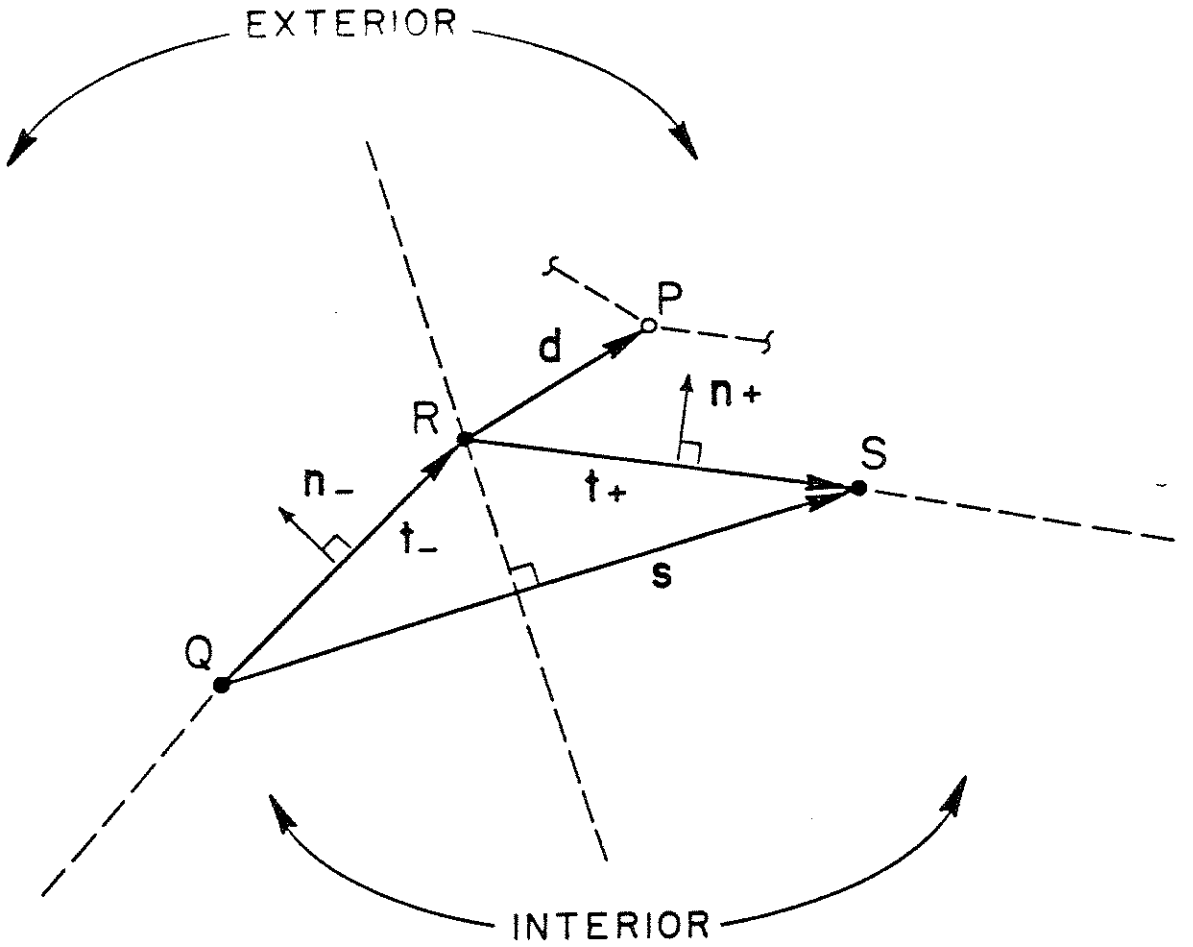

III-2 Typical configuration for candidate contact point (P) and target segment reference point (R).

straight lines emanating from R^i through Q^i and S^i and extending to infinity, and all points to the right of these lines with respect to the target direction. The exterior is the remaining portion of the plane (see Fig.III-2 for the analogous set-up for P,Q,R and S). At the end of an iteration, if P^i is in the interior of the target we say that tentative contact has been made. To determine if this has occurred we employ the following algorithm (see Fig. III-2 for notation). Let $\underset{\sim}{A}$ = (P;Q,R,S) and define "Test" as indicated in Fig III-3. If the outcome of "Test" is true (T) then P^i is exterior to the target, whereas if the outcome is false (F) P^i is in the interior and tentative contact has been made. In the latter case further calculations are required to determine if indeed contact has occurred* and, if so, where. This is dealt with in the next section.

* A candidate contact node can enter the interior without passing through the target, e.g., by "sneaking" around a boundary node.

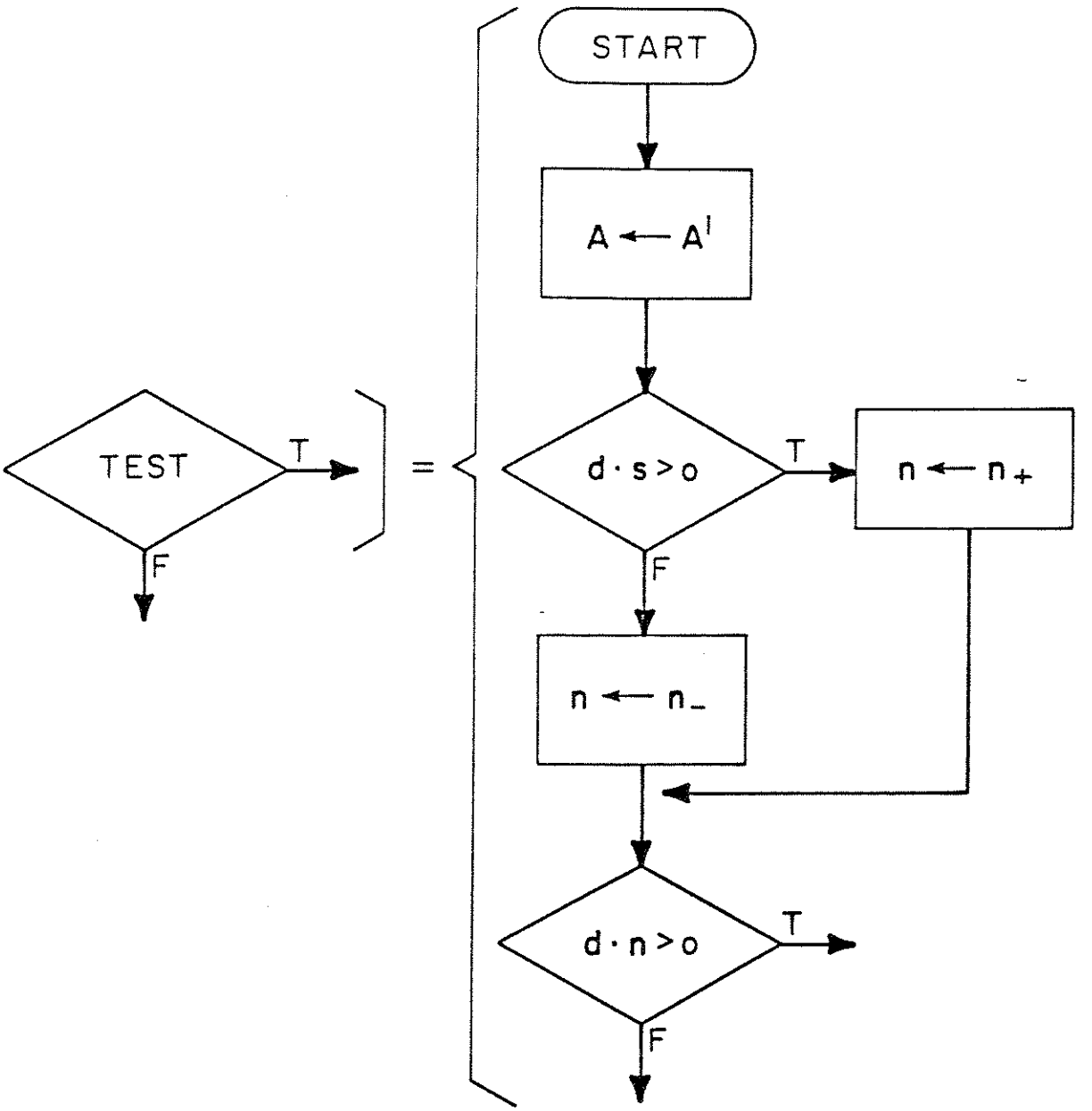

III-3 Test to decide if a candidate contact point is interior or exterior to the target.

3. Location of the Point of Initial Contact

Our technique for carrying out this calculation is best presented in a flowchart (see Fig. III-4). What follows is a brief description of the main steps. The routine requires the input parameters i_{max} and j_{max}, which are the maximum number of iterations allowed to determine the approximate location of a contact point, and the maximum number of changes of target reference node allowed, respectively. We loop on the candidate contact nodes $k=1,\ldots,N^1$ and extract ℓ, the nearest interior target node to k. Then we determine if tentative contact has been made. If this is the case we next employ a binary search procedure to determine a good approximation to the configuration ($\underset{\sim}{A}$) at which initial contact was actually made. With this configuration determined, we ascertain whether P actually contacted the segment QRS ($|\alpha| \leq 1$) or did not ($|\alpha| \geq 1$). In the former case we set up the tangent stiffness and right-hand side accordingly, whereas in the latter we may try another reference point and repeat the calculation. However, if the maximum number of changes of reference has been reached or the new reference point is a boundary point, we assume no contact has been made.

If it is determined that candidate contact node k is in contact, then we set the tangent stiffness for contactor k, target $\ell,\ell+1$ for the computed value of α. Compatibility is enforced by setting the right-hand side on the basis of $\underset{\sim}{A}^i$.

On the other hand, if it is determined that candidate contact node k is not in contact, then we set 1 in the appropriate diagonal element of the tangent stiffness and 0 in the right-hand side.

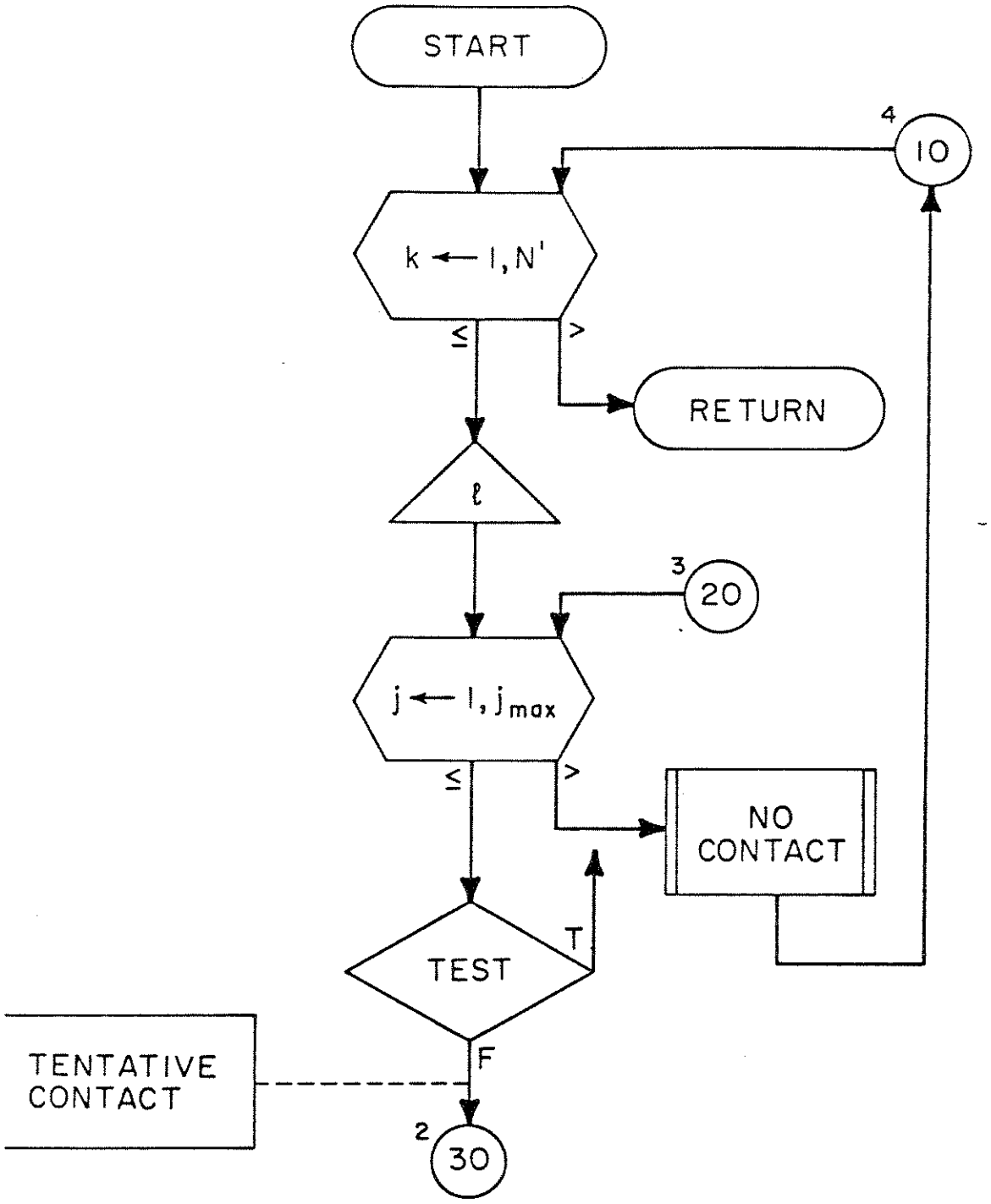

III-4 Flowchart for the kinematically nonlinear contact algorithm. Sheet 1/4.

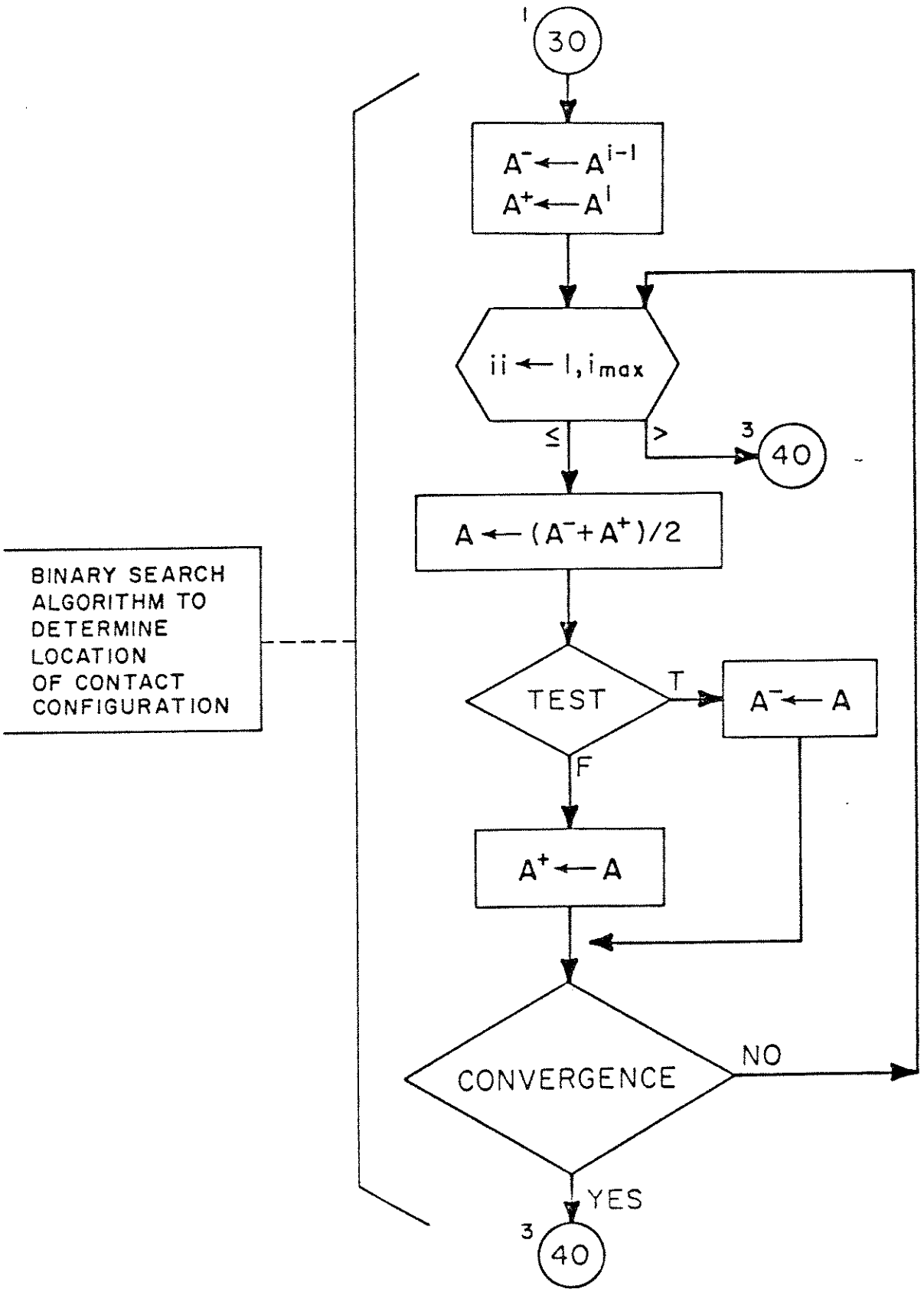

III-4 Flowchart for the kinematically nonlinear contact algorithm. Sheet 2/4.

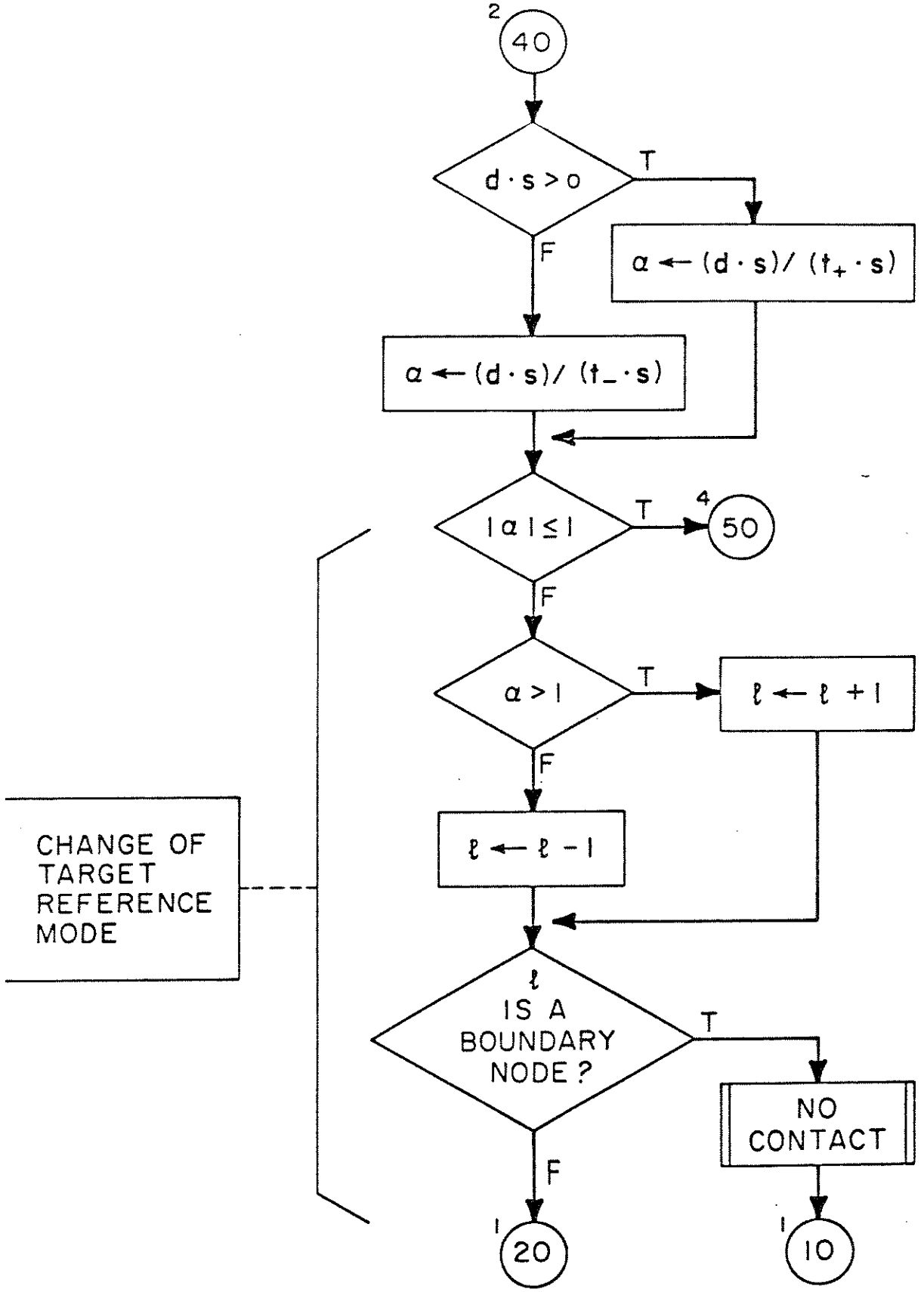

III-4 Flowchart for the kinematically nonlinear contact algorithm. Sheet 3/4.

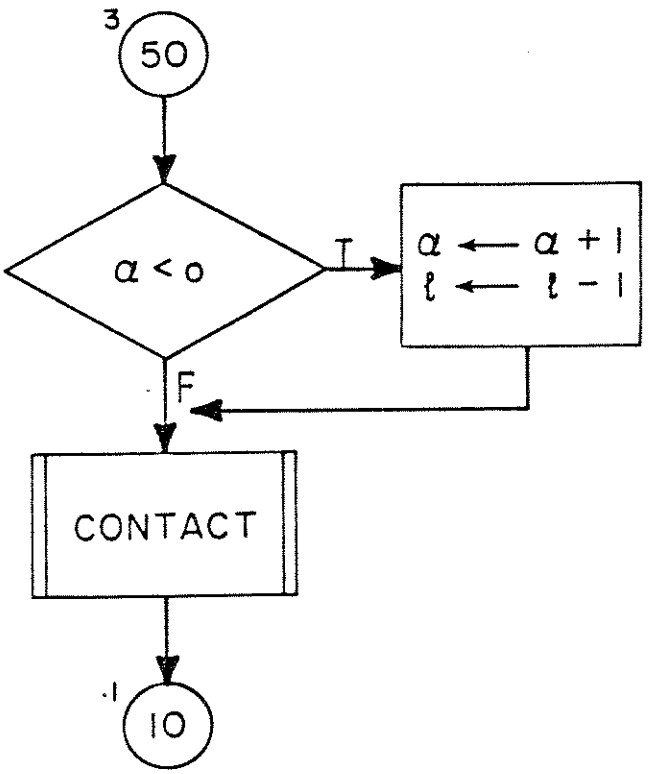

III-4 Flowchart for the kinematically nonlinear contact algorithm. Sheet 4/4.

IV. Fricitonal Contact Theory

In this section we present a very simple frictional contact theory. In subsequent progress reports we will describe an algorithm for this theory and its implemention in FEAP.

Assume the bodies B^1 and B^2, at a fixed time t, are in the configurations b^1 and b^2, respectively, and are in contact along c. Consider a point $\underset{\sim}{x}$ in c and let $\underset{\sim}{\tau}$ be the traction vector at $\underset{\sim}{x}$ with respect to b^1 (see Fig. IV-1). Let $\underset{\sim}{n}$ be the unit outward normal vector of b^1 at $\underset{\sim}{x}$. Since the bodies are in contact at $\underset{\sim}{x}$ we assume

$$\tau_n \overset{\text{def.}}{=} \underset{\sim}{\tau}\cdot\underset{\sim}{n} \leq 0, \text{ (compression)}.$$

The tangential part of $\underset{\sim}{\tau}$ is given by

$$\underset{\sim}{\tau}_s = \underset{\sim}{\tau} - \tau_n \underset{\sim}{n} \ .$$

We assume given a positive constant f called the coefficient of friction*. To simplify subsequent writing let

$$g = - f \tau_n \ ;$$

clearly $g \geq 0$. Define the relative tangential displacement and velocity of b^1 with respect to b^2, at $\underset{\sim}{x}$, by

$$\underset{\sim}{u}_s = \underset{\sim}{u}^1_s - \underset{\sim}{u}^2_s \ ,$$

$$\underset{\sim}{v}_s = \underset{\sim}{v}^1_s - \underset{\sim}{v}^2_s \ ,$$

respectively. With these definitions, Coulomb's theory of friction may

* f can depend on $\underset{\sim}{x}$ and t without essential complications.

be stated as follows (see [19]):

(i) Static case.

If $||\underset{\sim}{\tau}_s|| < g$, then $\underset{\sim}{u}_s = 0$.

If $||\underset{\sim}{\tau}_s|| = g$, then there exists a number $\lambda \geq 0$ such that $\underset{\sim}{u}_s = -\lambda \underset{\sim}{\tau}_s$ (i.e., $\underset{\sim}{u}_s$ points in the direction opposite $\underset{\sim}{\tau}_s$).

(ii) Dynamic case.

If $||\underset{\sim}{\tau}_s|| < g$, then $\underset{\sim}{v}_s = 0$.

If $||\underset{\sim}{\tau}_s|| = g$, then there exists a number $\lambda \geq 0$ such that $\underset{\sim}{v}_s = -\lambda \underset{\sim}{\tau}_s$.

Note that if f is formally taken to be $+\infty$, then Coulomb's theory corresponds to the perfect-friction (no-slip) case, whereas if f=0, then the theory reduces to the frictionless case.

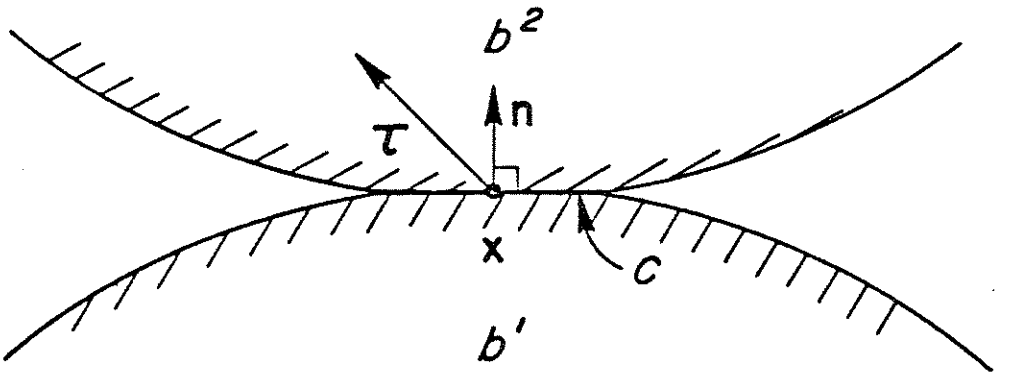

IV-1 Contact configuration.

References

1. T.J.R. Hughes, R.L. Taylor and J.L. Sackman, "Finite Element Formulation and Solution of Contact-Impact Problems in Continuum Mechanics." SESM Report No. 74-8, University of California, Berkeley (1974); copies can be obtained from National Technical Information Service, Springfield, Virginia, 22151, Accession No. PB-233 888/AS.

2. T.J.R. Hughes, R.L. Taylor and J.L. Sackman, "Finite Element Formulation and Solution of Contact-Impact Problems in Continuum Mechanics - II." SESM Report No. 75-3, University of California, Berkeley (1975).

3. T.J.R. Hughes, R.L. Taylor, J.L. Sackman, A. Curnier and W. Kanoknukulchai, "Finite Element Formulation and Solution of a Class of Contact-Impact Problems in Continuum Mechanics." To be presented at SMIRT Conference, London, Sept. (1975).

4. O.C. Zienkiewicz, The Finite Element Method in Engineering Science. McGraw-Hill, New York (1971).

5. C. Truesdell and W. Noll, "The Nonlinear Field Theories of Mechanics." In Handbuch der Physik, III/3. S. Flugge, editor. Springer, Berlin (1965).

6. L.R. Herrmann and R.M. Toms, "A Reformulation of the Elastic Field Equations in Terms of Displacements, Valid for all Admissible Values of Poisson's Ratio." J. Appl. Mech., 86, 140-141 (1964).

7. L.R. Herrmann, "Elasticity Equations for Incompressible and Nearly Incompressible Materials by a Variational Theorem." AIAA J., 3, 1896-1900 (1965).

8. R.L. Taylor, K.S. Pister and L.R. Herrmann, "On a Variational Theorem for Incompressible and Nearly-Incompressible Orthotropic Elasticity." Int. J. Solids Structures, 4, 875-883 (1968).

9. S.W. Key, "A Variational Principle for Incompressible and Nearly-Incompressible Anisotropic Elasticity." Int. J. Solids Structures, 5, 951-964 (1969).

10. T.J.R. Hughes and H. Allik, "Finite Elements for Compressible and Incompressible Continua." Proc. Symp. Civil Eng., Vanderbilt University, Nashville, Tenn., 27-62 (1969).

11. I. Fried, "Finite Element Analysis of Incompressible Material by Residual Energy Balancing." Int. J. Solids Structures, 10, 993-1002 (1974).

12. D.J. Naylor, "Stresses in Nearly Incompressible Materials by Finite Elements with Application to the Calculation of Excess Pore Pressures." Int. J. num. Meth. Engng, 8, 443-460 (1974).

13. J.T. Oden, Finite Elements of Nonlinear Continua. McGraw-Hill, New York (1972).

14. R.H. Iding, K.S. Pister and R.L. Taylor, "Identification of Nonlinear Elastic Solids by a Finite Element Method." Computer Methods in Applied Mechanics and Engineering, 4, 121-142 (1974).

15. J.H. Argyris, P.C. Dunne, T. Angelopoulos and B. Bichat, "Large Natural Strains and Some Special Difficulties Due to Nonlinearity and Incompressibility in Finite Elements." Computer Methods in Applied Mechanics and Engineering, 4, 219-278 (1974).

16. R.L. Taylor and J.L. Sackman, "Contact-Impact Models for Large Deformation Analysis." Proposal to: Civil Engineering Laboratory, Naval Construction Battalion Center, Port Hueneme, California, UCB-Eng-3889 (1974).

17. J.C. Nagtegaal, D.M. Parks and J.R. Rice, "On Numerically Accurate Finite Element Solutions in the Fully Plastic Range." Computer Methods in Applied Mechanics and Engineering, 4, 153-178 (1974).

18. O.C. Zienkiewicz, R.L. Taylor and J.M. Too, "Reduced Integration Technique in General Analysis of Plates and Shells." Int. J. num. Meth. Engng, 3, 275-290 (1971).

19. G. Duvaut and J.L. Lions, Les Inéquations en Mécanique et en Physique. Dunod, Paris (1972).

20. G.P. Cheupanov and E.F. Afanas'ev, "Some Dynamic Problems of the Theory of Elasticity - a Review." Int. J. Engng. Sci., 12, 665-690 (1974).

21. J.P. Wolfe, W.L. Hansen, E.E. Haller, R.S. Markiewicz, C. Kittel and C.D. Jeffries, "Photograph of an Electron-Hole Drop in Germanium." Physical Review Letters, 34, 1292-1293, (1974).

22. T.A. Shugar and M.G. Katona, "Development of Finite Element Head Injury Model." J. Engng Mechs Div., 101, 223-240 (1975).

23. S.W. Key, "A Finite Element Procedure for the Large Deformation Dynamic Response of Axisymmetric Solids." Computer Methods in Applied Mechanics and Engineering, 4, 195-218 (1974).